The nature of ferroelectricity under pressure

Igor A. Kornev* and Laurent Bellaiche

Physics Department, University of Arkansas, Fayetteville, Arkansas 72701, USA

(Dated: February 5, 2008)

Abstract

Advances in first-principles computational approaches have, over the past fifteen years, made possible the investigation of physical properties of ferroelectric systems. In particular, such approaches have led to a *microscopic* understanding of the occurrence of ferroelectricity in perovskite oxides at ambient pressure. In this paper, we report *ab-initio* studies on the effect of hydrostatic pressure on the ferroelectricity in perovskites and related materials. We found that, unlike commonly believed, these materials exhibit ferroelectricity at high enough pressure. We also explained in details the (unusual) nature of this ferroelectricity.

*Also at Novgorod State University, Russia; Electronic address: ikornev@uark.edu

I. INTRODUCTION.

ABO_3 perovskites form one of the most important classes of materials because they can exhibit a broad range of properties, e.g. superconductivity, magnetism, ferroelectricity, piezoelectricity, dielectricity and multiferroism. Such properties can be varied – and thus optimized to generate various devices with great performance and diverse functionalities – thanks to many factors. Examples of such factors are external magnetic and electrical fields, atomic substitution, chemical ordering and pressure.

In a classic paper (Samara *et al.*, 1975), Samara *at al.* were able to explain the effect of hydrostatic pressure on displacive phase transitions associated with soft zone-center transverse optic (TO) and zone-boundary phonons. Among the most striking pressure effects is the decrease of the transition temperature with pressure and ultimate vanishing of ferroelectricity (Samara *et al.*, 1975). As it was shown, the vanishing of ferroelectricity with pressure can be readily understood from the well-known soft-mode theory (Ginzburg, 2001) where the soft mode frequency depends on the short-range and Coulomb interactions. In this case, the vanishing of ferroelectricity is associated with a much more rapid increase of the short-range interactions than the long-range interactions with increasing pressure. As a result, the harmonic soft-mode frequency becomes less negative with increasing pressure. It is interesting to note that for the zone boundary modes the roles of the short-range and long-range forces are reversed, which leads to an enhancement of these modes when increasing pressure. Despite its simplicity, this model could successfully explain high pressure behavior of many compounds (Samara *et al.*, 1975; Sani *et al.*, 2004). [Note that "long-range" interactions denote interactions that persist even at distances where the electronic wavefunctions no longer overlap. Such long-range interactions have a distance dependency that is inversely proportional to some power of the interionic distance. "Short-range" interactions only occur when the electronic wavefunctions overlap. They typically have a distance dependency that follows an exponential form at large distances, and are inversely proportional to some power of the interionic distance at smaller distances.

The microscopic understanding of the occurrence of ferroelectricity in perovskite oxides has been substantially improved by first-principles electronic band-structure techniques. In particular, Cohen & Krakauer (Cohen, 1992; Cohen and Krakauer, 1990, 1992) showed that

a delicate balance exists between Coulomb interactions that favor ferroelectric distortions and the short-range repulsions that favor the undistorted high-symmetry structure. It it has been established that the balance between different competing interactions can be tipped by relatively small effects that are related to covalency, namely hybridization between p orbitals of the oxygen atoms and the d orbitals of the B atoms. In fact, such covalency is essential for stabilizing the ferroelectric distortion or, equivalently, triggers the soft-mode instability. The reason for this stabilization is that the hybridization weakens the short-range repulsions. This fact has been elegantly demonstrated by Posternak *et al.* (Posternak *et al.*, 1995) – who showed that the ferroelectric instability disappears in $KNbO_3$ when the interaction between the O $2p$ and Nb $4d$ states is artificially suppressed. Since then, similar conclusions have been drawn for other ferroelectric perovskites. Moreover, an additional Pb-O hybridization is the key factor to explain why $PbTiO_3$ has deeper ferroelectric double-well potentials than $BaTiO_3$ (Cohen and Krakauer, 1992; Kuroiwa *et al.*, 2001). The important role of covalent bonding is also clearly reflected in the anomalously large values of the Born dynamical charges (Ghosez *et al.*, 1998; Zhong *et al.*, 1994).

In this paper, we use first principles calculations to investigate many insulating perovskites and related materials under hydrostatic pressure, and show that the conclusion about the role of the different interactions mentioned above is indeed well justified at low pressure but is no longer valid at high pressure (Kornev *et al.*, 2005). More precisely, our study reveals (1) the *absence* of a cubic paraelectric phase in favor of a polar phase under high-enough hydrostatic pressures, and (2) the underlying physical mechanisms responsible for this overlooked phenomenon.

II. COMPUTATIONAL DETAILS.

The *ab initio* calculations are performed in the framework of the density functional theory, mostly within the local-density approximation (LDA) but also sometimes within the gradient generalized approximation (GGA) (Perdew and Yue, 1986; Perdew *et al.*, 1996). We have employed the pseudopotential method using the ABINIT (Gonze *et al.*, 2002), CUSP (Bellaiche and Vanderbilt, 2000; King-Smith and Vanderbilt, 1993), and PWscf (Baroni *et al.*, 2001) packages. The calculations have been done with the extended norm-conserving pseudopotentials of Teter (Teter, 1993) or with the Vanderbilt-type ultra-

soft pseudopotentials (Vanderbilt, 1990) – always incorporating the semi-core states in the valence, unless specified otherwise. The wavefunction has been expanded in planewaves up to a kinetic energy cutoff of 120 Rydberg when using the extended norm conserving pseudopotentials and of 40 Rydberg when using the ultrasoft pseudopotentials. We use the Ceperley-Alder exchange and correlation (Ceperley and Alder, 1980) as parameterized by Perdew and Zunger (Perdew and Zunger, 1981) or the Teter-Pade parametrization (Goedecker *et al.*, 1996; Perdew and Wang, 1992). For the ground state calculations, integrals over the simple cubic Brillouin zone have been replaced by sums on a 6 x 6 x 6 Monkhorst-Pack special k-point mesh (Monkhorst and Pack, 1976). We determined: (i) the total energy for different volumes of the unit cell allowing for full relaxation of the cell shape and the positions of the atoms inside the unit cell, in order to determine the evolution of some phases as a function of hydrostatic pressure, (ii) the phonon spectrum of specific structures by using both finite-difference (frozen-phonon) and linear-response approaches (Gonze *et al.*, 1992), (iii) the Born effective charges, the dielectric constants, and (iv) the electronic band-structure and density of states. It should be noted that we checked that our results are qualitatively independent on technical details such as the used exchange-correlation functional, pseudopotential types, kinetic energy cutoff or softwares.

III. RESULTS AND DISCUSSION

A. $PbTiO_3$ under pressure

Lead titanate $PbTiO_3$ is one of the most important and best studied ferroelectric materials adopting the simple-cubic perovskite structure at high temperature. It is known that $PbTiO_3$ undergoes a single ferroelectric transition from the cubic to a tetragonal phase below 766 K. In fact, it appears to be a textbook example of a displacive ferroelectric transition (Burns and Scott, 1973; Lines and Glass, 1977).

Hydrostatic pressure P reduces, and even annihilates for high enough value, ferroelectricity (FE) in perovskites (Sani *et al.*, 2004; Sanjurjo *et al.*, 1983), *according to the conventional theory*. Such annihilation seems consistent with experimental X-ray diffraction studies (Sani *et al.*, 2002; Zha *et al.*, 1992) and first-principles calculations (Wu and Cohen, 2005) that reported a ferroelectric to paraelectric phase transition in lead titanate under a

"moderate" (i.e. around 10-20 GPa) pressure. On the other hand, one of our recent studies (Kornev *et al.*, 2005) – that combines experimental techniques and *ab-initio* simulations – revealed that perovskites enhance their ferroelectricity as pressure increases *above a critical value* (which is around 30 GPa in PbTiO3).

More specifically, we performed 0 K calculations on $PbTiO_3$ within LDA and for a wide pressure range. The calculated pressure-volume data were fitted to a Birch equation of state (Birch, 1986). Here, we present the results for 7 phases: the *paraelectric* cubic $Pm\overline{3}m$ state; the *ferroelectric*, rhombohedral $R3m$, and tetragonal $P4mm$ phases; the *antiferrodistortive* tetragonal $I4/mcm$ and rhombohedral $R\overline{3}c$ phases; and the tetragonal $I4cm$ and rhombohedral $R3c$ phases that can exhibit *both* polar *and* antiferrodistortive degrees of freedom.

Figure 1*a* shows the predicted pressure dependency of the difference $\Delta H = H - H_{cubic}$ between the H_{cubic} enthalpy of the paraelectric cubic state and the H enthalpies of the other 6 phases. For the lowest (P) pressures, only ferroelectric distortions exist in $I4cm$ and $R3c$, which are thus identical to $P4mm$ and $R3m$, respectively. The $P4mm$ phase has the lowest ΔH, as consistent with the fact that it is the well-known ground state of $PbTiO_3$. Figs. 1(*b, c*) show that, as expected in perovskites (Samara *et al.*, 1975; Sani *et al.*, 2004), significant antiferrodistortive deformations occur in the $I4cm$ and $R3c$ phases when increasing P above ∼3 GPa. The reason leading to the TiO_6 octahedra rotation is clear: due to the TiO_6 octahedra rotation, the Ti-O bonds perpendicular to the rotational axis can relax towards their equilibrium lengths, which minimizes the bond compression. In other words, the rotation relaxes the compression of the Ti-O bond perpendicular to the rotational axis. On the other hand, Fig. 1 also indicates an unexpected result, namely that *increasing pressure above a critical value enhances ferroelectricity*! Indeed, an increase in P from 0 to ∼20 GPa leads to a ΔH becoming less negative in the polar phases - as consistent with the commonly-believed pressure-induced reduction of FE (Samara *et al.*, 1975; Sani *et al.*, 2004; Sanjurjo *et al.*, 1983), but the ΔH *–vs.-*P curve of these phases adopts an opposite behavior above P_c∼30 GPa - revealing that $PbTiO_3$ wants to become more and more ferroelectric after this critical pressure. We found that rhombohedral states are the most stable ones at high pressure (Kornev *et al.*, 2005) and at 0K. The non-monotonic behavior of FE versus pressure is emphasized by the pressure dependency of the calculated c/a axial ratio in P4mm (see Fig. 2): this ratio first strongly decreases with P until reaching a cubic-like value ∼1 in

the vicinity of P_c, and then it gradually increases as P further increases. Our predictions are thus in sharp contrast to the common expectation that the application of hydrostatic pressure favors a cubic paraelectric crystal structure.

B. Possible driving mechanism(s) for the high-pressure ferroelectric instability in $PbTiO_3$.

In order to identify the driving mechanism(s) of the ferroelectric instability under high pressure, we decided to investigate in more details (1) the cubic paraelectric $Pm\overline{3}m$ phase and (2) the tetragonal ferroelectric $P4mm$ phase. Fig. 1*b* shows that the magnitude of the polarization above the turning point is smaller than that below $\simeq$ 10GPa. Based on this fact, one *might* assume that the polarization is no longer the primary order parameter at high pressure or, equivalently, that the ferroelectric instability is driven by the coupling with other degrees of freedom, such as (i) the antiferrodistortive and (ii) elastic variables.

Possibility (i) is a primary suspect because antiferrodistortive degrees of freedom are known to increase with pressure in ferroelectric perovskites (Sani *et al.*, 2004). In this case, the ferroelectric instability could appear as a result of a specific interaction between the antiferrodistortive and ferroelectric distortions. However, these two degrees of freedom usually *compete* in perovskites (Vanderbilt and Zhong, 1998). Furthermore, as shown in Figure 1, the ferroelectric instability exists even without taking into account the antiferrodistortive degrees of freedom. For instance, after the turning point around $\simeq$ 30GPa, the $P4mm$ phase (that does not contain any rotation of the oxygen octahedra) is more stable than the cubic phase. These facts thus rule out the antiferrodistortive degrees of freedom to be the driven force for the ferroelectric instability.

Possibility (ii) is also a candidate for explaining high-pressure FE because perovskite ferroelectrics are well-known to exhibit a coupling between polarization and strain. An elastic *instability* may thus lead to the occurrence of a nonzero polarization. To check such hypothesis, we performed *ab initio* calculations of the elastic tensor in the cubic phase using the ABINIT package and found *no elastic instability* in the entire pressure range. Fig. 3 shows the pressure dependence of the elastic stiffness coefficients c_{11} , c_{12} , and c_{44}. The c_{11} and c_{12} coefficients increase linearly with increasing pressure. On the other hand, the c_{44} coefficient starts to decrease gradually above the critical pressure but remains positive at

all investigated pressures (that is, up to $\simeq$ 150 GPa) . Furthermore, these elastic stiffness coefficients satisfy the generalized elastic *stability* criteria for cubic crystals under hydrostatic pressure [see, for example, Ref. (Karki *et al.*, 1997)]: $c_{11} + 2c_{12} > 0$, $c_{11} - c_{12} > 0$, $c_{44} > 0$. Moreover, we found that the $P4mm$ phase *without* lattice relaxation is more stable at high pressure than the cubic phase. Therefore, we may now assume that the polarization *is* the primary order parameter even after the turning point. Elucidating the mechanisms of the high-pressure ferroelectric instability should thus involve the consideration of the soft transverse optical mode alone. (Note that we can also conclude that the electromechanical coupling that become enormous in the transition regions from the tetragonal to high pressure phases of $PbTiO_3$ (Cohen and Wu, 2006) is not responsible for the ferroelectric instability).

C. Lattice Dynamical Properties of $PbTiO_3$ and of Related Perovskites.

It is well-known that the Born effective charges are of primary interest for the soft TO mode behavior when a competition between the Coulomb and non-classical short-range forces is important. In the following, we will denote $O_{\parallel}$ the oxygen atoms located between two B-atoms along the z-direction and $O_{\perp}$ the oxygen atoms located between two B-atoms in the perpendicular directions – when slightly displacing the atoms along the z-axis when computing the Born effective charges. Our calculations of the Born effective charges as a function of pressure in the cubic phase (see Fig. 4) show that the anomalously large values of Ti and $O_{\parallel}$ persist throughout the pressure range of interest, although these effective charges decrease with increasing pressure For instance, their values are reduced by $\sim 1.4\%$ at ~ 25 GPa with respect to their values at 0GPa]. On the other hand, the effective charges of Pb and $O_{\perp}$ ions increase with pressure, and deviate from their values at zero pressure by $\sim 2\%$ at $\sim$ 25 GPa. Interestingly, it was demonstrated by Ghosez *et al.* (Ghosez *et al.*, 1996) that a change corresponding to a reduction of the order of 1% of the Ti effective charges is enough to suppress the ferroelectric instability in $BaTiO_3$. From this point of view, the tendency of the $PbTiO_3$ system to become cubic as the pressure first increases from zero is quite understandable. However, since after the turning point the Ti and $O_{\parallel}$ effective charges continue to decrease with pressure, one might expect that the system would continue to stay cubic *which is definitely not the case*. Therefore, the pressure behavior of the effective charges or, equivalently, the strengths of the Coulomb interaction *alone* is not sufficient to

understand high-pressure FE.

We now turn to Fig. 5*a* that displays the LDA-simulated pressure behavior of the zone-center transverse optical (TO) mode frequency in the cubic $Pm\overline{3}m$ phase of $PbTiO_3$. The square of such frequency is always negative, which indicates that $PbTiO_3$ has a ferroelectric instability and thus can not be cubic for any pressure at 0K. More importantly, the magnitude of this square first decreases with P and then increases above the critical pressure (P_c) - confirming that $PbTiO_3$ has to become more and more ferroelectric above P_c. To understand further the high-pressure ferroelectric instability it is advantageous to divide the dynamical matrix into (1) the Coulomb part (following the formalism for the rigid ion model) that can easily be found once the Born effective charges and dielectric tensor of the system have been calculated (Giannozzi *et al.*, 1991), and (2) the (remaining) second part – which is deduced by subtracting the first part from the total dynamical matrix. This second part thus differentiates the real material from its rigid ions picture, and gathers the (non-classical) short-range interactions. Figure 5*b* shows the calculated contribution of these two parts to the zone-center soft TO phonon frequency in the cubic phase of $PbTiO_3$ and $BaTiO_3$, as a function of P. Below P_c and as commonly expected (Samara *et al.*, 1975), the Coulomb interactions favor FE while short-range interactions tend to annihilate it - since they have a negative and positive frequency square, respectively - and the decrease of FE when increasing P is driven by the cost of short-range interactions becoming predominant over the gain associated with long-range interactions. Figure 5*b* also reveals that FE above P_c dramatically differs from the low-pressure "normal" ferroelectricity because of the *reverse* sign of Coulomb and short-range parts: it is now short-range effects (which are electronic in nature) that favor FE at high pressure while Coulomb interactions (that involve ions "dressed by electrons") prefer paraelectricity!

Figure 5*b* indicates that the results that we present are qualitatively general for perovskite ferroelectrics and not just an artifact of studying lead-contained perovskites, since they also apply to $BaTiO_3$. This fact is further emphasized in Figures 6 that report our 0 K *ab-initio* predictions for the eigenvalue λ and eigenvectors (ξ_A, ξ_B, $\xi_{O_\perp}$, $\xi_{O_\perp}$, $\xi_{O_\parallel}$) of the second-derivative matrix defined in Ref. (King-Smith and Vanderbilt, 1994) and associated with the soft-mode in cubic $PbTiO_3$, $BaTiO_3$ and $BaZrO_3$, as a function of pressure. (It is important to realize that the last two materials are *lead-free*). A *negative* λ corresponds to a ferroelectric instability while the magnitude of the eigenvectors quantifies the contribution of the different

ions to FE, if any. All the data displayed in Figs. 6 are obtained by using the local density approximation (LDA) except in parts (a) and (d) for which we also report results from the use of the generalized gradiant approximation (GGA). Figs. 6 undoubtedly show that *all* studied materials should be ferroelectric at high enough pressure, thus confirming that one has to rule out a possible suggestion that pressure-induced FE only occurs in Pb-based materials. One can further notice that ξ_A has a very small magnitude at high pressure in $PbTiO_3$, $BaTiO_3$ and $BaZrO_3$. This fact clearly implies that the A atoms contribute very little to high-pressure ferroelectricity. Our Figs. 6 also nicely summarize the different behaviors one can get as pressure increases in transition-metal perovskites, as a result of our discovered non-monotonic pressure behavior: the existence of FE at any pressure ($PbTiO_3$, see LDA calculation of Fig. 6(a)), the disappearance and then reentrance of FE under pressure ($BaTiO_3$, see Fig 6(b)), and the occurrence of FE at high pressure in a nominally paraelectric compound ($BaZrO_3$, see Fig. 6(c)). Moreover, Figures 6(d-f) clearly shows that the eigenvectors of B and O atoms have a large (and mostly material-independent!) magnitude at high pressure, which points to an "universal" microscopic explanation for high-pressure FE. Finally, such pressure-induced phenomenon is also found when performing *ab-initio* calculations in $KNbO_3$, $NaNbO_3$, $SrTiO_3$, $CaTiO_3$, as shown in Fig. 7, $Pb(Zr,Ti)O_3$ and some Bi-based perovskites (not shown here). Not also that the fact that the A atom contributes little to high-pressure FE is clearly confirmed in Fig. 8–that shows that A-free WO_3 material also enhances its FE at high enough pressure.

D. Electronic Structures under Pressure

We now resume our "detective" work and look for the microscopic origin of the observed high-pressure FE. As it was shown above, the instability is related to the non-classical short-range interactions. As a result, we will now mostly concentrate on *electronic* properties.

1. Influence of semicore states.

We first investigate the role played by the semicore states via Fig. 9 that shows the predicted pressure behavior of phonons in $PbTiO_3$ in the cubic phase *when neglecting to incorporate the semicore states of Pb and Ti as valence electrons.* Technically, the *ab-initio* sim-

ulations without the semicore states have been performed with the Troullier-Martins norm-conserving pseudopotentials within ABINIT. Fig. 9 indicates that the semicore states Pb $5d^{10}$ and Ti $3s^2 3p^6$ (1) must be included explicitly to produce the well-known ferroelectric instability at zero pressure – as consistent with previous first-principles works (Cohen and Krakauer, 1992; King-Smith and Vanderbilt, 1994) but (2) are *not* the reason for the existence of a turning point and of high-pressure FE (Note, however, that the magnitude of the instability is of course not the same when neglecting or incorporating these semicore states in the valence electrons). Note that the fact that Pb $5d^{10}$ orbitals are not responsible for the existence of the ferroelectric instability at high pressure could also have been guessed thanks to Fig. 8 that shows that tungsten trioxyde WO_3 (which is a defect-perovskite structure having *no* *A*-atom) also exhibits a highy-pressure FE. In fact, this latter figure, as well as Figs. (6,7), indicates that the electrons of interest for high-pressure FE should belong to the O and/or B ions.

2. Influence of the d-states of B atoms.

Figure 10 reports the LDA-predicted pressure behavior of the soft-mode eigenvalues of the second-derivative matrix in cubic bismuth aluminate $BiAlO_3$ and magnesium silicate $MgSiO_3$. Note that both materials, unlike the ones considered above, do not possess any B-atom having *occupied d* electrons. Interestingly, no turning point is observed in $MgSiO_3$ - under pressure up to 300 GPa. As a matter of fact, we found that the TO soft mode at the Γ point linearly increases with pressure in this material and become positives at around 30 GPa - which is consistent with previous studies of $MgSiO_3$ (Parlinski and Kawazoe, 2000). The same qualitative behavior is found in $BiAlO_3$ under high pressure up to 900 GPa. We thus arrive at the conclusion that the *d* states of the B atoms are of primary importance for understanding the physics behind the high-pressure ferroelectric instability.

3. Electronic band structure and density of states under pressure

To further elucidate the nature of the high-pressure ferroelectric instability and the role played by the electronic structure, we have calculated the total and atomic site projected densities of states (PDOS) of ideal cubic perovskites. Figs. 11 display some partial electronic

density of states for cubic $PbTiO_3$ under different pressures. Note that the contribution of Pb orbitals is not shown because, as discussed above, Pb was found to be relatively ferroelectric-inactive at high pressure.

Figures 11(*a*-*c*) show the low-lying states ranging between -22 and -15 eV (that solely originate from the O *2s* orbitals in an ionic picture), as well as the topmost group of valence bands (that exhibits the well-known hybridization between O *2p* and Ti *3d* orbitals (Cohen, 1992; Cohen and Krakauer, 1990)). As it is known, the topmost states correspond mainly to σ (bonding) and π (non-bonding) orbitals. Moreover, the states with large Ti $3d$ contribution are mainly concentrated in the lower (bonding) part of the topmost region. This O *2p* and Ti *3d* hybridization persists throughout the pressure range of interest. The integrated PDOS of this group have a smooth and small pressure-dependency thus ruling out that high-pressure FE is caused by this p – d hybridization. At the same time the Ti *3d* state contribution to the low-lying O *2s*-like bands has increased considerably. Thus, as the pressure increases, the admixture of Ti *3d* states in the occupied bands seems to evolve differently for the occupied low-lying and topmost bands. More precisely, the evolution of O $2s$ - Ti $3d$ and O $2p$ - Ti $3d$ mixing is nicely seen in the trends displayed by the *integrated* (over all the occupied valence bands) PDOS (to be denoted by IPDOS), see Fig. 12(*a*). The IPDOS of O $2s$ and Ti $3d$ vary in a correlated way with pressure, the former decreasing and the latter increasing. On the other hand, the IPDOS of O $2p$ remains more or less constant, apart from the highest pressures. These tendencies are even more clearly seen in Fig. 12(*b*), where IPDOS are normalized with respect to their corresponding values at zero pressure. Furthermore, Fig. 12(*c*) reports the contributions to the IPDOS coming from the low-lying states (located between -22 and -15 eV) and from the topmost group of the valence bands. The most striking effect is that Ti *3d* orbitals (and more precisely their e_g parts) dramatically increase (in a nonlinear way) their mixing with the O *2s* orbitals above P_c. The admixture of Ti $3d$ states in the occupied levels of the electronic structure releases O $2s$ - O $2s$ antibonding states above the Fermi level, thus optimizing the band energy. A similar behavior of integrated PDOS was found in $BaTiO_3$ under pressure, as reported in Fig. 13.

A rapid relative increase of the *O-s* and *B-d* mixing can easily be understood as follows. The lobes of the Ti $3d - t_{2g}$ orbitals point between the oxygen ligands (whereas the Ti $3d - e_g$ orbitals point directly towards the ligands), forming the σ bonding. Hence, the overlap with O $2s$ orbitals will be significant at high enough pressure for the Ti $3d - e_g$

states, which results in local repulsion between overlapping charge densities. From one hand, this repulsive interaction will cost some energy. From the other hand, some of the repulsion is compensated by hybridization in the resulting bonding states – which in turn leads to considerable amount of O $2s$ state in the conduction band. Taking into account the different interatomic dependence of these two competing interactions, one might expect that the need to avoid the large local repulsion will win at some pressure, enabling atomic distortions and thus giving rise to ferroelectricity.

We would like to point out that the important role played by the small amount of $2s$ admixture with the e_g orbitals of transition-metal cations surrounded by anions (like chlorine, bromine, fluorine, or oxygen) was also previously recognized in Ref. (Moreno *et al.*, 1997). Moreover, recent DFT calculations (Hussermann, 2003) revealed the key role of $s-d$ mixing on the stability of high-pressure structures in P, As, Sb, and Bi.

E. Topological analysis of the electron density in $PbTiO_3$.

To get more insight into the chemical bondings of $PbTiO_3$ under pressure, we consider the topological properties of the electron density $\rho(r)$. The *total* density was restored by adding atomic core electron density to the valence density obtained in pseudopotential calculations. The analysis was performed in terms of the atom-in-molecules Bader theory (Bader, 1990) which is based upon the so-called critical points, r_{cp}, of the electron density. At these points, the gradient of the electronic density is null and the Hessian matrix $\partial^2\rho(r)/\partial x_i \partial x_j$ is characterized by its three eigenvalues, λ_k. Interatomic interactions can be adequately described by the topological properties of the electron density at the so-called (3,-1) critical points (or bond critical points) for which the three eigenvalues of the Hessian matrix are non-zero and the algebraic sum of their signs is -1. Bond critical points occur as saddle points along bond paths between pairs of bonded atoms and can be used to define atomic coordination. The characteristics of the bond critical points in $PbTiO_3$ at 0 GPa are listed in Table 1.

As expected for cubic perovskite [see, for instance, Ref. (Zhurova and Tsirelson, 2002)], we found six (3,-1) critical points on the Ti-O lines and twelve (3,-1) critical points on the Pb-O lines at any pressure. Interestingly, all the (3, -1) critical points in $PbTiO_3$ are characterized by the positive Laplacian of the electron density which, according to Bader (Bader,

TABLE I Characteristics of some critical points (CP) in $PbTiO_3$ at $a = 7.35$ *a.u.* (zero pressure); $\nabla^2\rho(r_{cp}) = \lambda_1 + \lambda_2 + \lambda_3$, where λ_1 and λ_2 are perpendicular to the bond line curvatures of the electron density and λ_3 is parallel. Values are given in atomic units.

r_{cp}	$\rho(r_{cp})$	$\nabla^2\rho(r_{cp})$	λ_1	λ_2	λ_3	Type of CP
$(0.234, 1/2, 1/2)^a$	0.132	0.590	-0.219	-0.219	1.028	(3,-1)
$(0, 0.267, 0.267)^b$	0.028	0.078	-0.020	-0.022	0.120	(3,-1)

[a]Ti-O line.
[b]Pb-O line.

1990), is an indication of the closed-shell interaction between the corresponding atoms.

Analyzing the topological characteristics available in the literature, it was found (Zhurova and Tsirelson, 2002) that the bonds, typically identified as *ionic*, are characterized by the electron density value at the (3,-1) critical point in the range of 0.07–0.25 e $Å^{-3}$ and a specific range of the ratio of the perpendicular and parallel curvatures of the electron density: $0.12 < |\lambda_1|/\lambda_3 < 0.17$. According to Table I, the Pb-O bond (at 0 GPa) fits well the first condition since $\rho(r_{cp}) \approx 0.1908$ e $Å^{-3}$ and closely fits the second one if we take $|(\lambda_1 + \lambda_2)/2|/\lambda_3 \approx 0.176$ rather than $|\lambda_1|/\lambda_3$. Thus, the Pb-O interaction (at zero pressure) can be considered as mostly ionic with small covalent admixture. On the other hand, the value of $\rho(r_{cp}) \approx 0.9$ e $Å^{-3}$ and the ratio $|\lambda_1|/\lambda_3 = 0.213$ at the (3,-1) critical points on the Ti-O line imply that the Ti-O bond is *not* ionic in nature (at zero pressure).

In order to characterize the chemical bonds in more details (and for different pressures), we employ the recently proposed classification scheme of interatomic interactions (Espinosa *et al.*, 2002). According to Bader (Bader, 1990) the Laplacian function $\nabla^2\rho(r_{cp})$ is related to the potential energy density $v(r_{cp})$ (of negative value) – which represents the capacity of the system to concentrate electrons at the critical point – and the kinetic energy density $g(r_{cp})$ (of positive value) – which gives the tendency of the system to dilute electrons at the same point (Espinosa *et al.*, 1998) – through the local form of the virial theorem $1/4\nabla^2\rho(r_{cp}) = 2g(r_{cp}) + v(r_{cp})$. Note that for pressure different from zero, the virial theorem should include an additional term proportional to this P pressure: in the cubic case, one should add the $+3P$ term to the lefthand side of this latter expression.

The kinetic energy can be calculated using the following expression for closed-shell in-

teractions at the bond critical points (Abramov, 1997): $g(r_{cp}) = 3/10(3\pi^2)^{2/3}\rho(r_{cp})^{5/3} + 1/6\nabla^2\rho(r_{cp})$. The potential energy density $v(r_{cp})$ is then calculated by subtracting $g(r_{cp})$ from $1/4\nabla^2\rho(r_{cp})$. We also computed the total electronic energy density $h(r)$ at the r_{cp} points as $h(r_{cp}) = g(r_{cp}) + v(r_{cp})$. Using the adimensional $|v(r_{cp})|/g(r_{cp})$ ratio and the bond degree $BD = h(r_{cp})/\rho(r_{cp})$, the atomic interactions can be divided into three classes (Espinosa *et al.*, 1998): (i) pure closed shell for which $|v(r_{cp})|/g(r_{cp}) < 1$ (and for which the $\nabla^2\rho(r_{cp}) > 0$ and $h(r_{cp}) > 0$ inequalities stand), (ii) pure shared shell for which $1 < |v(r_{cp})|/g(r_{cp}) < 2$ (and for which $\nabla^2\rho(r_{cp}) < 0$ and $h(r_{cp}) < 0$) and (iii) transit closed shell for which $|v(r_{cp})|/g(r_{cp}) > 2$ (with $\nabla^2\rho(r_{cp}) > 0$ and $h(r_{cp}) < 0$).

Inside the ionic region (i), the bond degree parameter is an index of ionicity: the stronger the ionicity the greater the BD magnitude. In regions (ii) and (iii), the BD parameter measures the covalency degree: the stronger the covalency the greater the BD magnitude. For instance, the ionic Li-F bond is characterized by $|v(r_{cp})|/g(r_{cp}) \approx 0.76$ and $BD \approx +0.41$ while the covalent C-O bond in $CO(NH_2)_2$ is such as $|v(r_{cp})|/g(r_{cp}) \approx 2.64$ and $BD \approx -0.29$ (Tsirelson, 2002). Fig. 14 reports the bond degree parameter versus $|v(r_{cp})|/g(r_{cp})$ ratio (as determined from our first-principles calculations) for the Ti-O and Pb-O bonds. This figure confirms that the Pb-O bond lies close to the pure closed shell region (i.e., it is mostly ionic) at 0GPa, and reveals that such bond becomes more ionic at higher pressure. On the other hand, the Ti-O bond lies close to the middle of a transit region (ii), implying that the Ti-O bond is neither purely covalent nor purely ionic. Fig. 14 also shows that the covalency degree of the Ti-O bond increases with pressure, which is consistent with our band structure calculations discussed above in subsection D.3. Interestingly, since this covalency increases with pressure, there might be a possibility for the phase transition to occur due to the drastic collapse of the oxygen *ionic* size (which is related to charge transfer to oxygen). For example, the Shannon ionic radius of O^{2-} is 1.23 Å (Shannon, 1976), whereas its covalent radius is 0.73 Å (Sanderson, 1962). If the size of oxygens were small compared to the allowed space then the oxygen atoms would be weakly bounded in the lattice and a multi-well potential could be expected [similar to PbTe:Ge (Murase, 1980; Weiser, 1981) and $PbTe_{1-x}S_x$ (Abdullin *et al.*, 1984)]. The mechanism for the off-center instability of the O ion could be viewed in this case as an imbalance between the decreased (due to small O radius) repulsive forces and the polarization forces that tend to displace the ion from its position. Furthermore, the on-site force constant of the O ion would become negative

and the O ion would be unstable to the displacement from its regular high symmetry site with local distortions. This would lead to the instability of O similar to one observed for Li in $LiNbO_3$ (Parlinski *et al.*, 2000). Indeed, although we found that the so-called Bader volumes (Bader, 1990; Gonze *et al.*, 2002) (which are a measure of the ionic volumes) are smooth functions over the pressure interval of interest, the Bader O volume, unlike those of Pb and Ti, decreases faster under pressure than the volume of the unit cell, as shown in Fig. 15. However, our *ab initio* lattice vibration calculations show that the on-site force constant of O is *positive* at any pressures and, hence, the local atomic potential possesses a single minimum. We thus can rule out the drastic collapse of the oxygen ionic size as the mechanism for the high-pressure ferroelectricity.

F. Simple Tight-Binding Model

To confirm the role of the interaction between the $2s$ orbitals of oxygen atoms and the d orbitals of the B atoms at high pressure, we use the bond-orbital model of Harrison (Harrison, 1980) – a simplified tight-binding model, where the Hamiltonian is limited to the on-site and nearest-neighbor terms. This approximation allows an extraordinary simplification of the problem and the total energy can be rigorously calculated bond by bond. This is a very crude approximation but, surprisingly, it works very well in a wide variety of systems. In particular, it explains reasonably well the dynamical charges in ferroelectric perovskites (Ghosez *et al.*, 1998). In this section, we shall make use of the method to clarify the role of the O $2s$ – B d and O $2p$ – B d couplings in the high pressure ferroelectric instability in perovskites. We will see that the instability at high pressure is governed by a competition between short-range covalent and overlap interactions.

Intuitively, the gradually decreasing ferroelectricity with rising hydrostatic pressure from zero to small values (i.e., before the turning point) may be attributed to the fact that the conventional mechanism responsible for triggering the ferroelectric instability at zero pressure and related to the B d – O $2p$ hybridization is not working well under pressure because of an increase of covalency. It is known that in the case of significantly covalent systems a paraelectric phase is of lower energy than the ferroelectric one due to the increasing of the rigidity and the stability of the metal-oxygen network (Villesuzanne *et al.*, 1998). From this point of view, it seems likely that – besides the pd covalency that appears to

prevent the ferroelectric instability at high pressure – there is an interaction that reveals itself only at high enough pressure (i.e., when the distance between atoms is sufficiently small). This gives us a clue that the interaction should be small at large interatomic distances (e.g., at zero pressure) and should increase more rapidly than covalency effects at small interatomic distances, bringing the ferroelectric instability into the system.

For a qualitative understanding of phase transformations under pressure, we recall that two energy contributions to the cohesive energy, namely the covalent and overlap energies, depend most strongly on the interatomic distance. According to the Harrison model, the (attractive) covalent interaction depends on the interatomic distance, d, as $\sim d^{-7/2}$ while the (repulsive) overlap interaction – which is due to nonorthogonality of wave functions on adjacent sites – behaves as $\sim d^{-7}$ and thus depends more strongly on the nearest-neighbor distance. The interplay between the short-range covalent and the overlap interactions can be nicely seen from the following arguments. The covalent energy contribution mainly represents the short-range electron-ion potential energy while the overlap energy can be predominantly ascribed to the increase of the kinetic energy of the valence electrons upon compression (Harrison, 1986). Since the resulting forces due to these two interactions (central repulsive forces and covalent forces) scale differently under pressure, one might expect that at some pressure the noncentral nature of the bonding will become negligible. Indeed, Fig. 16 shows that the high-pressure Cauchy relation between the elastic constants for hydrostatic conditions $C_{12} = C_{44} + 2P$, where C_{12} and C_{44} are the elastic constants calculated from first-principles, is satisfied for cubic $PbTiO_3$ in the vicinity of the the turning point ($\simeq$ 30GPa), which indicates an insignificant role of noncentral and many-body forces in this pressure region. This fact implies that, for instance, empirical two-body potentials could be used for calculations of elastic properties for pressures around the turning point. Away from the critical pressure the deviation from the Cauchy relation becomes significant. The latter implies that the contribution of either noncentral or many-body forces becomes more and more important at higher pressures, and it cannot be treated anymore as a small correction to the two-body potentials. Thus, we clearly see manifestation of the competing forces under pressure.

Note that a major role of competition between covalent and overlap interactions has been recognized for *sp*-bonded solids (Majewski and Vogl, 1985). Remarkably, a drastic softening of the transverse optical phonons across the pressure-induced phase transition

was predicted, and the physical origin of this softening was shown to be closely related to ferroelectricity (Majewski and Vogl, 1987).

Let us now proceed further by approximating, in Ti-based perovskites, the total effect of the coupling (i) between the oxygen $2s$ states and the d-orbitals of the Ti atom, and (ii) between the oxygen $2p$ states and the d-orbitals of the Ti atom, via the following expressions:

$$\begin{aligned} E_{sd\ bond} &= 2V_3(sd) - 2[V_2(sd)^2 + V_3(sd)^2]^{1/2} + E_{sd\ rep} \\ E_{pd\ bond} &= 6V_3(pd) - 6[V_2(pd)^2 + V_3(pd)^2]^{1/2} + E_{pd\ rep} \end{aligned} \tag{1}$$

where the (polar energies) V_3 are the average of the cation and anion energy, and are given by $V_3(sd) = (e_d - e_s)/2$ and $V_3(pd) = (e_d - e_p)/2$ – with $e_s = -29.14$ eV, $e_p = -14.13$ eV, and $e_d = -11.04$ eV (which are the energies of the $2s$ and $2p$ states of the oxygen atom and of the $3d$ states of the titanium atom, respectively (Harrison, 1980). The second terms $[...]^{1/2}$(which are the covalent energies) are connected with the bond formation energy and are responsible for lowering the energy of the bonding state. Based upon a second-moment approximation (Wills and Harrison, 1983), these covalent energies are given by $V_2(sd)^2 = \sum_j V_{sd\sigma}(r_j)^2$ and $V_2(pd)^2 = \sum_j (V_{pd\sigma}(r_j)^2 + 2V_{pd\pi}(r_j)^2)/3$, where the last sum is over the 6 nearest neighbors to Ti and where the so-called Harrison's two-center interactions, V_{ldm}, can be taken to be of the form (Harrison, 1980):

$$V_{ldm} = \eta_{ldm} \frac{\hbar^2}{\mu} \frac{r_d^{3/2}}{r_j^{7/2}} \tag{2}$$

where r_j is the interatomic distance between Ti and the j^{th} nearest-neighbor O, μ is the free-electron mass, $r_d = 1.029$ Å for titanium, $m = \sigma, \pi$, and η's take the following values: $\eta_{sd\sigma} = -3.16$, $\eta_{sd\sigma} = -2.95$, and $\eta_{sd\sigma} = 1.36$ (Harrison, 1980).

The third terms of Eq. (1), $E_{sd\ rep}$ and $E_{pd\ rep}$, are related to the overlap interactions. A repulsion comes from the shift in the energy of each electron due to the nonorthogonality of the s, d and p, d states on adjacent sites, with the average shifts being given by (Harrison and Straub, 1987):

$$\begin{aligned} \delta\varepsilon_{sd} &= -\sum_j V_{sd\sigma}(r_j) S_{sd\sigma}(r_j) \\ \delta\varepsilon_{pd} &= -1/3 \sum_j [V_{pd\sigma}(r_j) S_{pd\sigma}(r_j) + 2V_{pd\pi}(r_j) S_{pd\pi}(r_j)] \end{aligned} \tag{3}$$

The overlap repulsion for a given bond, is equal to this shift times the number of electrons in these states. In the approximations adopted here we use the extended Hückel theory (Hoffmann, 1963) to derive the overlap elements, as proposed by van Schilfgaarde and Harrison (van Schilfgaarde and Harrison, 1986). It is plausible to take the overlap elements to be proportional to the corresponding off-diagonal hopping elements and inversely proportional to the on-site atomic orbital energies: $S_{\alpha dm}(r) = \frac{2}{K_{\alpha d}} V_{\alpha dm}(r)/(e_\alpha + e_d)$, where $\alpha = s, p$ and $m = \sigma, \pi$. For the Wolfsberg-Helmholz parameter $K_{\alpha d}$, the weighted formula $K_{\alpha d} = \kappa + (e_\alpha - e_d)^2/(e_\alpha + e_d)^2 + (1-\kappa)(e_\alpha - e_d)^4/(e_\alpha + e_d)^4$ (Ammeter *et al.*, 1978) could be used. In general, the Wolfsberg-Helmholz parameter $K_{\alpha d}$ can be given by the distance-dependent form (Calzaferri and Rytz, 1996). For the sake of simplicity and following Refs. (Baranowski, 1984; Harrison, 1983; Majewski and Vogl, 1987), we assume that K takes a different value for each row of the Periodic Table, i.e., the K of Carbon ($K_C = 1.63$) for Oxygen and the K of Ge ($K_{Ge} = 1.07$) for Titanium (Harrison, 1999) and take the average as $K = (K_C K_{Ge})^{1/2}$.

Following this scheme, the covalent or polar bonding character of a given bond (e.g., *sd* or *pd*) can now be addressed. For each bond, the bond polarity, α_p, of the compound can be obtained from $\alpha_p^2 = V_3^2/(V_2^2 + V_3^2)$ and a complementary quantity, the covalency coefficient, α_c, is defined through the relation $\alpha_c^2 = 1 - \alpha_p^2$. The tight-binding model demonstrates the strong reduction of the *polarity* of the *sd* and *pd* bonds under pressure, as shown in Fig. 17. On the other hand, the model predict a considerable increase of the *sd* $O - Ti$ chemical bond covalency under pressure (i.e., when the interatomic distance decreases) – which is consistent with the first-principles population analysis reported in Section III.D.3. Indeed, as it can be clearly seen from Fig. 17, the *sd* bond covalency depends more strongly on the nearest-neighbor distance than the *pd* bond covalency, and therefore the first one may predominantly determine the behavior of perovskites in the vicinity of the turning point.

In the Harrison bond-orbital formalism, the frequency of the $q = 0$ optical phonon can be easily obtained (Harrison, 1980). Consider a perovskite structure viewed along a $\langle 100 \rangle$ direction with a relative displacement $u_j = u_{Ti} - u_{O_j}$ of the Ti and O atoms from their equilibrium positions in a $\langle 100 \rangle$ direction when the atoms oscillate according to a Γ-point soft mode. Accordingly, the change in length of the indicated bond $Ti-O$ is δd_j, leading to a change in the bonding energy of $\delta E_{sd\ bond}$ and $\delta E_{pd\ bond}$. These changes in the bonding energy may be viewed as the frozen-phonon energy obtained as the difference of the respective energy

relative to its equilibrium value, $\delta E_{\alpha d\ bond} = E_{\alpha d\ bond}(u_j) - E_{\alpha d\ bond}(0)$. For the evaluation of the *sd* and *pd* contributions to the frozen-phonon energy, usual harmonic fit function can be used, i.e. $2\ \delta E_{\alpha d\ bond} = \omega_{\alpha d}^2 \sum_j M_j u_j^2$, where M_j are the atomic masses, and $\omega_{\alpha d}$ are the contributions from *sd* and *pd* interactions to the total frequency. [As an alternative to the above method, an analytic expression for these changes can be obtained by expanding Eq. 1 in a Taylor series with respect to the displacements and then truncating the series to the second order in the displacements.]

Let us consider the frequency of the $q = 0$ optical mode in which the Ti and O atoms move out of phase with the relative displacements which reproduce a high-pressure eigenvector of the soft mode obtained from first-principles (see, e.g., Fig.6). Since above the turning point the relative displacement of each of the 4 transverse oxygens $u_\perp$ is greater than that of each of the 2 longitudinal oxygens $u_\parallel$, $2u_\perp > u_\parallel$, we have chosen the following displacement pattern along the z axis for the 6 oxygen ions: $[0.4u, 0.4u, u, u, u, u]$ with $u = 0.002$. Denoting d as half of the cubic lattice constant We now see that one neighbor distance becomes $d - 0.4u$ (between the Ti atom and the top O atom), one becomes $d + 0.4u$ (between the Ti atom and the bottom O atom) and four become $(d^2 + u^2)^{1/2}$ (between the Ti atom and 4 transverse O atoms).

The results of the frozen-phonon calculations are shown in Fig. 18. At large interatomic distances both *sd* and *pd* contributions stabilize the paraelectric state, since they both have a *positive* δE. The curves of $\delta E_{sd\ bond}$ and $\delta E_{pd\ bond}$ have maximums which lies at around 2 $\mathring{A}$ and 1.8 $\mathring{A}$, respectively. One thus finds a maximum at around 1.85 $\mathring{A}$ for the sum of two contributions. [Note that the experimental equilibrium interatomic distance in, for instance, $SrTiO_3$ is 1.95 $\mathring{A}$ and the turning point is around 1.85 $\mathring{A}$ according to our first-principles calculations.] These estimates are compatible with the assumption that the repulsion overlap energy does not become important until the turning point. The most striking result is that the model predicts a strong phonon softening upon compression since Fig. 18 shows that both $\delta E_{sd\ bond}$ and $\delta E_{pd\ bond}$, that first increase with pressure and reach a maximum at around the turning point, then decrease rapidly under compression and become negative at ≈ 1.83 $\mathring{A}$ and ≈ 1.6 $\mathring{A}$, respectively. The interatomic distance at which the sum of both contributions becomes negative is ≈ 1.64 $\mathring{A}$, to be compared with our *ab-initio* result of ≈ 1.78 $\mathring{A}$ for $SrTiO_3$. [It should be emphasized that an exact agreement with *ab-initio* calculations cannot be expected, on account of the approximations made in

the tight-binding model, especially the neglect of long-range interaction.] Interestingly, it is the *sd* contribution which first destabilizes the paraelectric phase under the influence of pressure. Therefore, the phonon frequency is reduced under pressure after the turning point as much as this destabilization is not compensated for by the other energy contributions. Moreover and interestingly, as the system is further compressed the *pd* contribution also contributes to the destabilizing of the parelectric phase. The present tigh-binding model thus predicts a striking softening of a Γ-point phonon mode under compression, and clearly explains the strong preference of perovskites to form ferroelectrically distorted structures at high pressure due to an *electronically driven* structural instability (i.e., electron-phonon coupling). In particular, this simple model reveals the predominant role played by the costly-in-energy overlap between the $2s$ orbitals of oxygen and the $3d$ orbitals of Ti on the high-pressure FE of perovskites.

G. Electronically Driven Instability

According to the above simple tight-binding model, it is the electrons and their interactions with ions (i.e., electron-phonon coupling) that are responsible for the high-pressure ferroelectric instability of perovskites. In this section, the electron-ion interaction will be considered in more details. More precisely, we shall be interested in the electronic contribution into the ferroelectric soft mode within DFT and within the adiabatic approximation.

Note that the adiabatic approximation consists in (a) neglecting the phonon contributions to the electronic density response and (b) approximating the dynamical response by a static one (Geilikman, 1975; Sham, 1974). In the adiabatic approximation, the electrons are considered to remain in the instantaneous (electronic) ground state when the lattice vibrates. Consequently, the effect of electrons on the adiabatic phonon frequencies is due to the fact that the change in the charge density induced by the displacements of nuclei screens the external perturbation (and the linear-response equations must be solved self-consistently) (Savrasov, 1996).

To refresh readers' memory, let us remind some basic equation of density-functional theory (DFT). Within the framework of DFT, the total energy can be expressed in terms of the Kohn-Sham eigenvalues ϵ_i:

$$E = \sum_i f_i \epsilon_i - \frac{e^2}{2} \int d\mathbf{r} d\mathbf{r}' \frac{n(\mathbf{r}) n(\mathbf{r}')}{|\mathbf{r} - \mathbf{r}'|} + E_{xc}[n(\mathbf{r})] - \int n(\mathbf{r}) v_{xc}(\mathbf{r}) d\mathbf{r} + E_N(\mathbf{R}). \quad (4)$$

where f_i is the occupancy of the state i, and $n(\mathbf{r})$ is the density of the valence electrons. The first term is the band structure energy:

$$\sum_i f_i \epsilon_i = \sum_i f_i \langle i | -1/2\nabla^2 + V_{SCF}(\mathbf{r}) | i \rangle \quad (5)$$

where an effective potential (also called *self-consistent*, SCF, potential) is:

$$V_{SCF}(\mathbf{r}) = V_{ext}(\mathbf{r}) + e^2 \int \frac{n(\mathbf{r}')}{|\mathbf{r} - \mathbf{r}'|} d\mathbf{r}' + v_{xc}(\mathbf{r}), \quad (6)$$

and $v_{xc}(\mathbf{r}) \equiv \delta E_{xc} / \delta n(\mathbf{r})$ is the exchange-correlation potential and $V_{ext}(\mathbf{r})$ is the external (ionic) potential acting on the electrons. $E_N(\mathbf{R})$ is the electrostatic interaction between different nuclei:

$$E_N(\mathbf{R}) = \frac{e^2}{2} \sum_{I \neq J} \frac{Z_I Z_J}{|\mathbf{R}_I - \mathbf{R}_J|}. \quad (7)$$

Note that, in general, the bare ion-ion contribution into phonon modes can stabilize as well as destabilize the paraelectric state. The destabilizing nature of this contribution is a trivial consequence of Earnshaw's theorem (Earnshaw, 1842; Feynman and Sands, 1975) that states that a static system of electric charges can *not* have a position of stable equilibrium. A a result, the crystals stability is ensured by the electron contribution to the force constants. Although it is possible that the ion-ion contribution to a ferroelectric soft mode destabilizes this mode, it is not necessarily the case – implying that the ferroelectric soft mode can be stable in a lattice of bare ionic charges (Kvyatkovskii and Maksimov, 1988). This particular situation occurs in the case of the ferroelectric soft mode in perovskites under pressure, since we numerically found that the ionic term in the force constants (which arises from the ion-ion Ewald term (Giannozzi *et al.*, 1991) with the bare ionic (pseudo)charges (for example, $Z_{Pb} = 14, Z_{Ti} = 12, Z_O = 6$)) is positive in the pressure range of interest.

Next, we are interested in the electronic contribution to the phonon spectrum. The total second-order change in the electronic energy $E_{el}^{(2)}$ can be written as (Johnson, 1969; Sham, 1969).

$$E_{el}^{(2)} \;=\; E_{el1}^{(2)} + E_{el2}^{(2)}$$

$$= \sum_{i \neq j} \frac{f_i \langle i|\delta V_{ext}|j\rangle\langle j|\delta V_{ext}|i\rangle}{(\epsilon_i - \epsilon_j)} + \sum_i f_i \langle i|\delta V^{(2)}_{ext}|i\rangle$$
$$= 1/2 \int d\mathbf{r}\delta n(\mathbf{r})\delta V_{ext}(\mathbf{r}) + \int d\mathbf{r} n^0(\mathbf{r})\delta V^{(2)}_{ext}(\mathbf{r}) \quad (8)$$

where $n^0(\mathbf{r})$ is the electronic density of the unperturbed crystal, $\delta n(\mathbf{r})$ is the change in the electron density due to the ionic displacements, $\delta V_{ext}(\mathbf{r})$ is the change in the "bare" potential experienced by the electron system to first order in the ionic displacements, and $\delta V^{(2)}_{ext}(\mathbf{r})$ the second order change. Therefore, the expression for the electronic contribution to the adiabatic force constant matrix consists of a negative-definite contribution $E^{(2)}_{el1}$ (the first term in Eq. 8) and a positive-definite contribution $E^{(2)}_{el2}$ (the second term in Eq. 8) (Kvyatkovskii and Maksimov, 1988).

Let us now consider the negative-definite contribution $E^{(2)}_{el1}$ to the adiabatic force constant matrix in more details (Geilikman, 1975; Kvyatkovskii and Maksimov, 1988). This contribution describes how a first order change in the external Hamiltonian leads to a first order change in the density matrix, which acts back at the Hamiltonian.

Let us first consider the change in density $\delta n(\mathbf{r})$ induced by a change in the external potential $\delta V_{ext}(\mathbf{r})$. Within DFT, one can define the non-interacting electron polarizability, $\chi_0(\mathbf{r}, \mathbf{r}')$, as the charge-density response to a variation of the total potential:

$$\delta n(\mathbf{r}) = \int d\mathbf{r}' \; \chi_0(\mathbf{r}, \mathbf{r}') \; \delta V_{SCF}(\mathbf{r}'). \quad (9)$$

The expression for $\chi_0(\mathbf{r}, \mathbf{r}')$ has the well known form (Pick *et al.*, 1970; Sham, 1969, 1974):

$$\chi_0(\mathbf{r}, \mathbf{r}') = \sum_{i,j} \frac{f_i - f_j}{\epsilon_i - \epsilon_j} \; \psi^*_i(\mathbf{r})\psi_j(\mathbf{r})\psi^*_j(\mathbf{r}')\psi_i(\mathbf{r}') \quad (10)$$

where the sums over i and j extend to both occupied and empty states. Clearly, only terms involving virtual transitions from occupied or partially occupied to empty or partially empty states contribute because of the difference $f_i - f_j$ in the numerator.

Recall the relationship between the bare and the self-consistent perturbing potential:

$$\delta V_{SCF}(\mathbf{r}) = \delta V_{ext}(\mathbf{r}) + \int d\mathbf{r}' \; K(\mathbf{r}, \mathbf{r}')\delta n(\mathbf{r}'), \quad (11)$$

where:

$$K(\mathbf{r}, \mathbf{r}') = \frac{e^2}{|\mathbf{r} - \mathbf{r}'|} + \frac{\delta^2 E_{xc}}{\delta n(\mathbf{r})\delta n(\mathbf{r}')}, \quad (12)$$

Combining Eqs. (8–11), one can rewrite the the negative-definite contribution as follows:

$$E_{el1}^{(2)} = 1/2 \int d\mathbf{r}\ \delta n(\mathbf{r}) \delta V_{ext}(\mathbf{r})$$
$$= 1/2 \int d\mathbf{r} d\mathbf{r}' \delta V_{SCF}(\mathbf{r}) \chi_0(\mathbf{r},\mathbf{r}') \delta V_{SCF}(\mathbf{r}') - 1/2 \int d\mathbf{r}'\ \delta n(\mathbf{r}) K(\mathbf{r},\mathbf{r}') \delta n(\mathbf{r}') \quad (13)$$

Substituting the results (12) and (13) in Eq. (8) we obtain

$$E_{el}^{(2)} = 1/2 \int d\mathbf{r} d\mathbf{r}' \delta V_{SCF}(\mathbf{r}) \chi_0(\mathbf{r},\mathbf{r}') \delta V_{SCF}(\mathbf{r}') + \int d\mathbf{r} n^0(\mathbf{r}) \delta V_{ext}^{(2)}(\mathbf{r})$$
$$- 1/2 \int d\mathbf{r}'\ \delta n(\mathbf{r}) \left[\frac{e^2}{|\mathbf{r}-\mathbf{r}'|} + \frac{\delta^2 E_{xc}}{\delta n(\mathbf{r}) \delta n(\mathbf{r}')} \right] \delta n(\mathbf{r}') \quad (14)$$

The first two terms in Eq. (14) are due to the variation of the band energy term in the total energy (the first term in Eq. (4)) and the third term in Eq. (14) is due to the variation of the Hartree energy and the exchange-correlation energy.

The total electronic contribution (see Eq. 8) to the interatomic force constant tensor $\Phi_{ll'}^{\alpha\beta}$ between the atoms at $\mathbf{r}_l$ and $\mathbf{r}_{l'}$ can be linked to the second-order change in the electronic energy with respect to collective ionic displacements in the usual way as $2E_{el}^{(2)} = \sum_{l,l'} \Phi_{ll'}^{\alpha\beta} u_{l,\alpha} u_{l',\beta}$, where $u_{l,\alpha}$ is the displacement of the lth ion in the α-direction from its equilibrium position $\mathbf{R}_l$.

Taking into account that $\delta V_{SCF}(\mathbf{r}) = \sum_l \delta V_{SCF}(\mathbf{r}) / \delta \mathbf{R}_l \cdot \mathbf{u}_l$, the negative-definite contribution of the band structure energy $E_{el1}^{(2)}$ to the dynamical matrix can be written in the form (Varma and Weber, 1979)

$$\Phi_{ll'}^{\alpha\beta}(\mathbf{q}) = \frac{1}{N_c} \sum_{\lambda\lambda',\mathbf{k}} \frac{f_{\mathbf{k}+\mathbf{q}\lambda'} - f_{\mathbf{k}\lambda}}{\epsilon_{\mathbf{k}+\mathbf{q}\lambda'} - \epsilon_{\mathbf{k}\lambda}}\ g_{\mathbf{k}+\mathbf{q}\lambda',\mathbf{k}\lambda}^{l\alpha *} g_{\mathbf{k}+\mathbf{q}\lambda',\mathbf{k}\lambda}^{l'\beta} \quad (15)$$

where N_c the number of unit cells in the crystal, and $g_{\mathbf{k}'\lambda',\mathbf{k}\lambda}^{l} = \langle \mathbf{k}'\lambda' | \delta V_{SCF}(\mathbf{r}) / \delta \mathbf{R}_{l\mathbf{q}} | \mathbf{k}\lambda \rangle$ are the electron-phonon matrix-elements. The sum has to be carried out, in principle, over all bands λ,λ' and all k points $\mathbf{k}$, $\mathbf{k}'$ that can be connected via the phonon wave vector $\mathbf{q}$. Interestingly, simplifying the electron-phonon matrix-elements within nonorthogonal tight-binding representation as (Varma and Weber, 1977, 1979) $g_{\mathbf{k}\lambda,\mathbf{k}'\lambda'} \propto (\partial \epsilon_{\mathbf{k}\lambda} / \partial \mathbf{k} [A_{\mathbf{k}}^\dagger S_{\mathbf{k}} A_{\mathbf{k}'}^\dagger]_{\lambda\lambda'} - \partial \epsilon_{\mathbf{k}'\lambda'} / \partial \mathbf{k}' [A_{\mathbf{k}}^\dagger S_{\mathbf{k}'} A_{\mathbf{k}'}^\dagger]_{\lambda\lambda'})$ – where S is the overlap and A the eigenvector matrix – we clearly see the dependence of the electron-phonon interaction on the overlap effects. An important feature of this expression noted in Refs. (Varma and Weber,

1977, 1979) is the fact that the electron-phonon coupling is large where the electron velocities are large and therefore the density of states are small. Indeed, we numerically checked these facts in our first principles calculations.

Interestingly, Eq. (15) is in fact the electron-phonon coupling in the so-called Fröhlich model (Frohlich, 1954) – which thus proves that such coupling is naturally included in the adiabatic approximation within DFT (Geilikman, 1975; Kvyatkovskii and Maksimov, 1988). (Note that the electron-phonon coupling is responsible for the ferroelectric instability in the vibronic theory of ferroelectricity (Kristoffel and Konsin, 1988), i.e., the existence of the pseudo Jahn-Teller effect due to the existence of two closely situated filled p and d empty bands in perovskites-like structures (Sinha and Sinha, 1964)).

Eq. (15) has been used to calculate the electron-phonon contribution to the ferroelectric soft mode at the Γ point in $PbTiO_3$ and $NaNbO_3$. More precisely, we obtained the eigenvalues of the LDA-determined $\Phi_{ll'}^{\alpha\beta}(\mathbf{q})$ matrix corresponding to the LDA-determined eigenvectors of the total dynamical matrix. The resulting eigenvalue ω_{ep}^2 corresponding to the soft TO mode is negative for any pressure and shown in Fig. 19, and clearly behaves in a nonmonotonic way with pressure. Interestingly, this nonmonotonic behavior varies in a correlated way with the soft-mode total frequency (see Figs. 6, 7, 8) under pressure– which thus confirms that the electron-phonon coupling is the leading mechanism for the high-pressure ferroelectricity.

IV. CONCLUDING REMARKS.

In summary, our results reveal that, unlike commonly thought, ferroelectricity is not suppressed by high pressure in insulating perovskites. Instead, ferroelectricity is found to enhance as pressure increases above a critical value. Moreover, this unexpected high-pressure ferroelectricity is different in nature from conventional ferroelectricity because it is driven by an original electronic effect rather by long-range ionic interactions. Depending on the energetic difference between ferroelectric and paraelectric phases at atmospheric pressure, such phenomenon can lead to various overlooked/original effects, e.g. (i) the disappearance and then re-entrance of ferroelectricity under pressure; (ii) the occurrence of FE at high pressure in a nominally-paraelectric compound; and (iii) the existence of FE at any pressure (see Figure 6). We thus hope that this article, and its numerous details, will stimulate the

investigation of novel effects in "smart" materials under pressure.

We would like to thank S. Prosandeev and I. Ponomareva for useful discussions. This work is supported by ONR grants N00014-01-1-0365, N00014-04-1-0413 and N00014-01-1-0600, by NSF grants DMR-0404335, and by DOE grant DE-FG02-05ER46188.

References

Abdullin, K., A. Lebedev, A. Gas'kov, V. Demin, and V. Zlomanov, 1984, JETP Lett. **40**(6), 998.

Abramov, Y., 1997, Acta Cryst. **A53**, 264.

Ammeter, J. H., H. B. Buergi, J. C. Thibeault, and R. Hoffmann, 1978, J. Am. Chem. Soc. **100**, 3686.

Bader, R., 1990, *Atoms in molecules. A quantum theory* (Oxford University Press, Oxford, UK).

Baranowski, J. M., 1984, J. Phys. C: Solid State Phys. **17**, 6287.

Baroni, S., A. Dal Corso, S. de Gironcoli, P. Giannozzi, C. Cavazzoni, G. Ballabio, S. Scandolo, G. Chiarotti, P. Focher, A. Pasquarello, K. Laasonen, A. Trave, *et al.*, 2001, (www.pwscf.org).

Bellaiche, L., and D. Vanderbilt, 2000, Phys. Rev. B **61**(12), 7877.

Birch, F., 1986, J. Geophys. Res. **91**(B5), 4949.

Burns, G., and B. Scott, 1973, Phys. Rev. B **7**(7), 3088.

Calzaferri, G., and R. Rytz, 1996, J. Phys. Chem. **100**, 11122.

Ceperley, D., and B. Alder, 1980, Phys. Rev. Lett. **45**(7), 566.

Cohen, R., 1992, Nature **358**(6382), 136.

Cohen, R., and H. Krakauer, 1990, Phys. Rev. B **42**(10), 6416.

Cohen, R., and H. Krakauer, 1992, Ferroelectrics **136**(1-4), 65.

Cohen, R., and Z. Wu, 2006, in *APS March Meeting* (Baltimore, MD).

Earnshaw, S., 1842, Trans. Camb. Phil. Soc. **7**, 97.

Espinosa, E., I. Alkorta, J. Elguero, and E. Molins, 1998, Chem. Phys. Lett. **285**, 170.

Espinosa, E., I. Alkorta, J. Elguero, and E. Molins, 2002, J. Chem. Phys. **117**, 5529.

Feynman, R., R.P.and Leighton, and M. Sands, 1975, *The Feynman Lectures on Physics*, volume 2 (Addison-Wesley).

Frohlich, H., 1954, Advances in Physics **3**(11), 325.

Geilikman, B., 1975, Sov. Phys. Usp. **18**, 190.

Ghosez, P., X. Gonze, and J. Michenaud, 1996, Europhysics Letters **33**(9), 713.

Ghosez, P., J.-P. Michenaud, and X. Gonze, 1998, Phys. Rev. B **58**(10), 6224.

Giannozzi, P., S. de Gironcoli, P. Pavone, and S. Baroni, 1991, Phys. Rev. B **43**(9), 7231.

Ginzburg, V., 2001, Phys-Usp. **44**, 1037.

Goedecker, S., M. Teter, and J. Hutter, 1996, Phys. Rev. B **54**(3), 1703.

Gonze, X., D. Allan, and M. Teter, 1992, Phys. Rev. Lett. **68**(24), 3603.

Gonze, X., J.-M. Beuken, R. Caracas, F. Detraux, M. Fuchs, G.-M. Rignanese, L. Sindic, M. Verstraete, G. Zerah, F. Jollet, M. Torrent, A. Roy, *et al.*, 2002, Computational Materials Science **25**(3), 478.

Harrison, W., 1980, *Electronic structure and the properties of solids : the physics of the chemical bond* (W. H. Freeman and Company, San Francisco).

Harrison, W., 1999, *Electronic Structure and the Properties of Solids* (River Edge, NJ : World Scientific, Singapore).

Harrison, W. A., 1983, Phys. Rev. B **27**, 3592.

Harrison, W. A., 1986, Phys. Rev. B **34**(4), 2787.

Harrison, W. A., and G. K. Straub, 1987, Phys. Rev. B **36**(5), 2695.

Hoffmann, R., 1963, The Journal of Chemical Physics **39**(6), 1397.

Hussermann, U., 2003, Chem. Eur. J. **9**, 1472.

Johnson, F. A., 1969, Proc. R. Soc. London Ser. A **310**, 79, 89, 101, 111.

Karki, B. B., G. J. Ackland, and J. Crain, 1997, J. Phys.: Condens. Matter **9**(41), 8579.

King-Smith, R., and D. Vanderbilt, 1994, Phys. Rev. B **49**, 5828.

King-Smith, R. D., and D. Vanderbilt, 1993, Phys. Rev. B **47**(3), 1651.

Kornev, I. A., L. Bellaiche, P. Bouvier, P.-E. Janolin, B. Dkhil, and J. Kreisel, 2005, Physical Review Letters **95**(19), 196804.

Kristoffel, N., and P. Konsin, 1988, Phys. Status Solidi B **149**(1), 11 .

Kuroiwa, Y., S. Aoyagi, A. Sawada, J. Harada, E. Nishibori, M. Takata, and M. Sakata, 2001, Phys. Rev. Lett. **87**(21), 217601.

Kvyatkovskii, O. E., and E. G. Maksimov, 1988, Sov. Phys. Usp. **31**, 1.

Lines, M. E., and A. M. Glass, 1977, *Principles and Applications of Ferroelectrics and Related Materials* (Clarendon Press).

Majewski, J., and P. Vogl, 1985, Phys. Rev. Lett. **57**(11), 1366.

Majewski, J., and P. Vogl, 1987, Phys. Rev. B **35**, 9666.

Monkhorst, H. J., and J. D. Pack, 1976, Phys. Rev. B **13**(12), 5188.

Moreno, M., J. A. Aramburu, and M. T. Barriuso, 1997, Phys. Rev. B **56**(22), 14423.

Murase, K., 1980, J. Phys. Soc. Jpn. **49**, 725.

Parlinski, K., and Y. Kawazoe, 2000, Eur. Phys. J. B **16**(1), 49.

Parlinski, K., Z. Q. Li, and Y. Kawazoe, 2000, Phys. Rev. B **61**(1), 272.

Perdew, J., and Y. Wang, 1992, Phys. Rev. B **45**(23), 13244.

Perdew, J., and W. Yue, 1986, Phys. Rev. B **33**, 8800.

Perdew, J., and A. Zunger, 1981, Phys. Rev. B **23**(10), 5048.

Perdew, J. P., K. Burke, and M. Ernzerhof, 1996, Phys. Rev. Lett. **77**(18), 3865.

Pick, R., M. H. Cohen, and R. Martin, 1970, Phys. Rev. B **1**, 910.

Posternak, M., R. Resta, and A. Baldereschi, 1995, Phys. Rev. B **50**(12), 8911.

Samara, G. A., T. Sakudo, and K. Yoshimitsu, 1975, Phys. Rev. Lett. **35**(26), 1767.

Sanderson, R., 1962, *Chemical Periodicity* (Reinhold, New York).

Sani, A., M. Hanfland, and D. Levy, 2002, J. Phys.: Cond. Matt. **44**, 10601.

Sani, A., B. Noheda, I. A. Kornev, L. Bellaiche, P. Bouvier, and J. Kreisel, 2004, Phys. Rev. B **69**(2), 020105.

Sanjurjo, J., E. Lopez-Cruz, and G. Burns, 1983, Phys. Rev. B **28**, 7260 .

Savrasov, S. Y., 1996, Phys. Rev. B **54**(23), 16470.

van Schilfgaarde, M., and W. A. Harrison, 1986, Phys. Rev. B **33**(4), 2653.

Sham, L. J., 1969, Phys. Rev. **188**(3), 1431.

Sham, L. J., 1974, *Theory of lattice dynamics of covalent crystals* (American Elsevier Publishing Cmpany, Inc., North-Holland, Amsterdam), volume 1 of *Dynamical Properties of Solids*, chapter 5, p. 301.

Shannon, R., 1976, Acta Cryst. **A32**, 751.

Sinha, K. P., and A. P. B. Sinha, 1964, Indian Journal of Pure and Applied Physics **2**(3), 91 .

Teter, M., 1993, Phys. Rev. B **48**(8), 5031.

Tsirelson, V. G., 2002, Acta Cryst. **B58**, 632.

Vanderbilt, D., 1990, Phys. Rev. B **41**, 7892.

Vanderbilt, D., and W. Zhong, 1998, Ferroelectrics **207**(1-2), 181 , ISSN 0015-0193.

Varma, C. M., and W. Weber, 1977, Phys. Rev. Lett. **39**(17), 1094.

Varma, C. M., and W. Weber, 1979, Phys. Rev. B **19**(12), 6142.

Villesuzanne, A., C. Elissalde, M. Pouchard, and J. Ravez, 1998, Eur. Phys. J. B **6**(3), 307.

Weiser, K., 1981, Phys. Rev. B **23**(6), 2741.

Wills, J. M., and W. A. Harrison, 1983, Phys. Rev. B **28**, 4363.

Wu, Z., and R. E. Cohen, 2005, Physical Review Letters **95**(3), 037601 (pages 4).

Zha, C., A. Kalinichev, J. Bass, C. Suchicital, and D. Payne, 1992, J. Appl. Phys. **72**(8), 3705.

Zhong, W., R. D. King-Smith, and D. Vanderbilt, 1994, Phys. Rev. Lett. **72**(22), 3618.

Zhong, W., D. Vanderbilt, and K. Rabe, 1995, Phys. Rev. B **52**(9), 6301.

Zhurova, E. A., and V. G. Tsirelson, 2002, **B58**, 567.

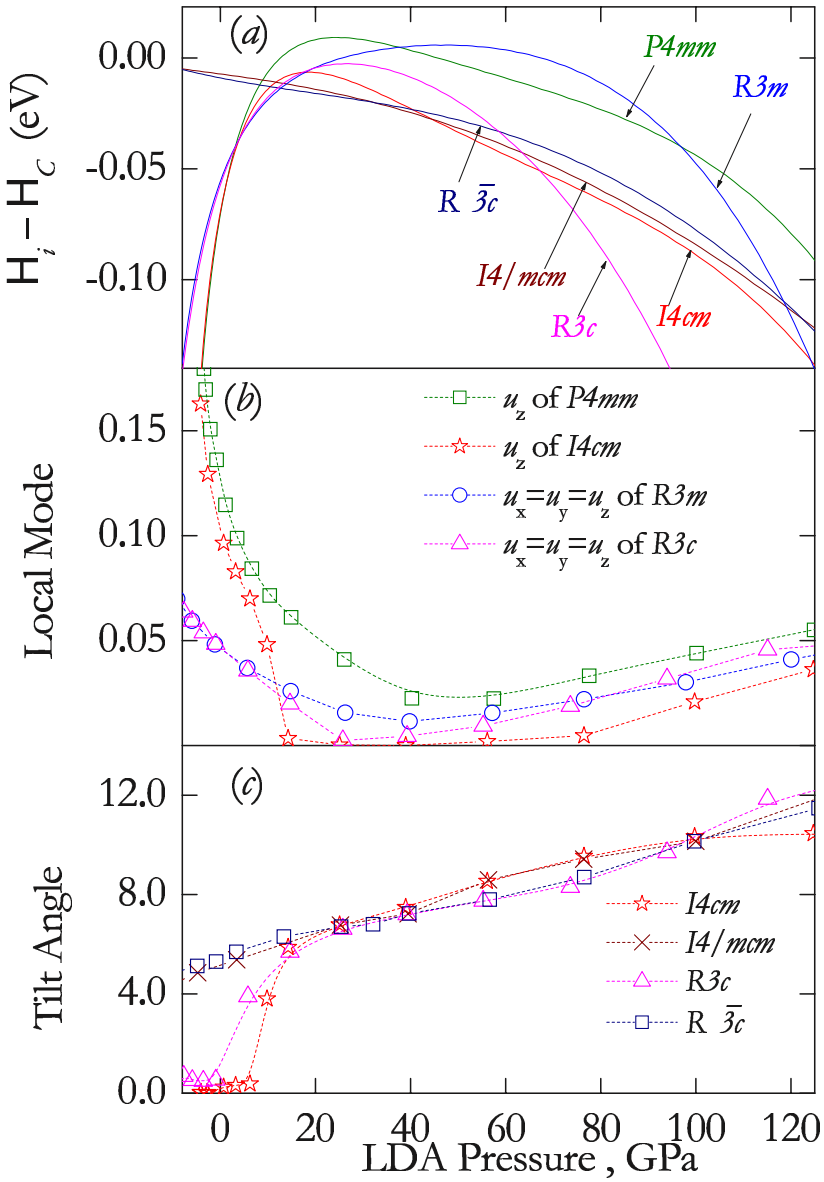

FIG. 1 First-principles prediction of the pressure behavior of (a) $\Delta\mathcal{H}$ (see text) for all the considered phases (the phase corresponding to a minimal $\Delta\mathcal{H}$ at a given P is thus the most stable one for this pressure), (b) the Cartesian components (along the pseudo-cubic $\langle 001 \rangle$ axes) of the polar local soft-mode (Zhong *et al.*, 1995) - which is directly proportional to the spontaneous polarization - for the P4mm, I4cm, R3m and R3c phases, and (c) the rotational angle of the oxygen octahedra with respect to the pseudo-cubic $\langle 111 \rangle$ direction for the R3c and R$\bar{3}$c rhombohedral phases and with respect to the pseudo-cubic $\langle 001 \rangle$ direction for the I4cm and I4/mcm tetragonal phases.

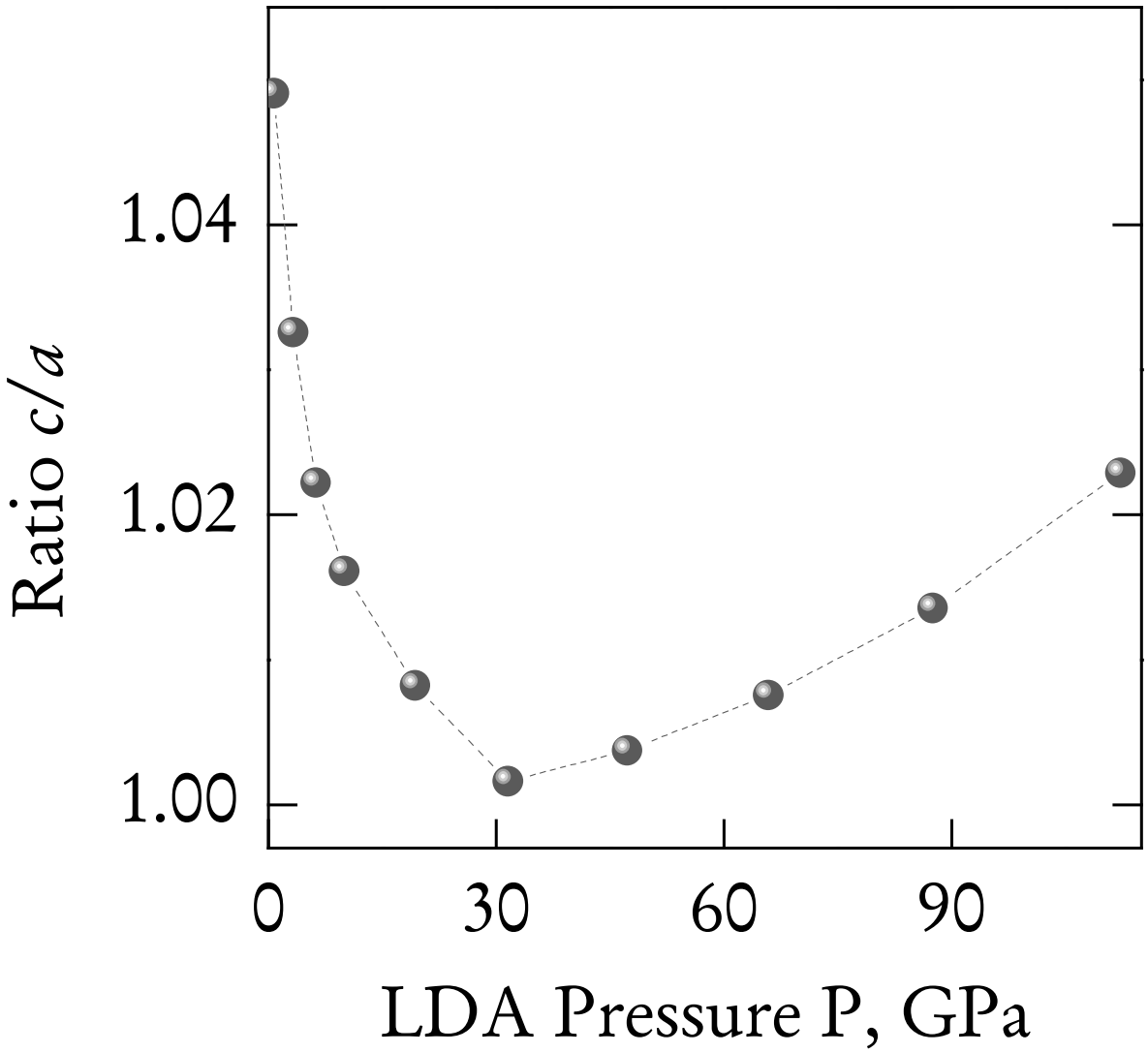

FIG. 2 The LDA-predicted pressure behavior of the c/a distortion at 0K for the P4mm phase in $PbTiO_3$.

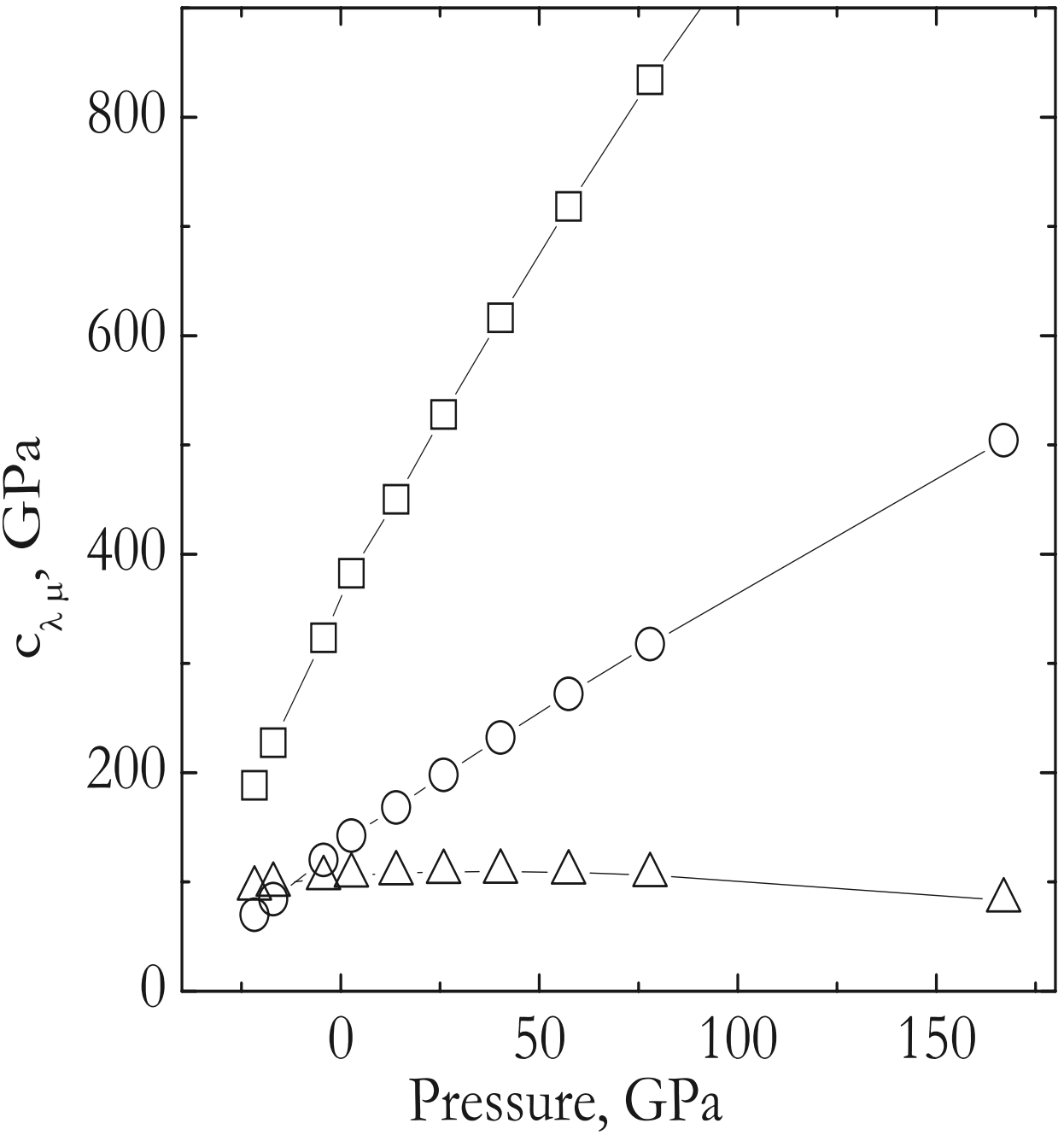

FIG. 3 The pressure dependence of the elastic stiffness coefficients c_{11} (squares), c_{12} (dots) , and c_{44} (triangles) of the cubic phase of $PbTiO_3$, as predicted by LDA.

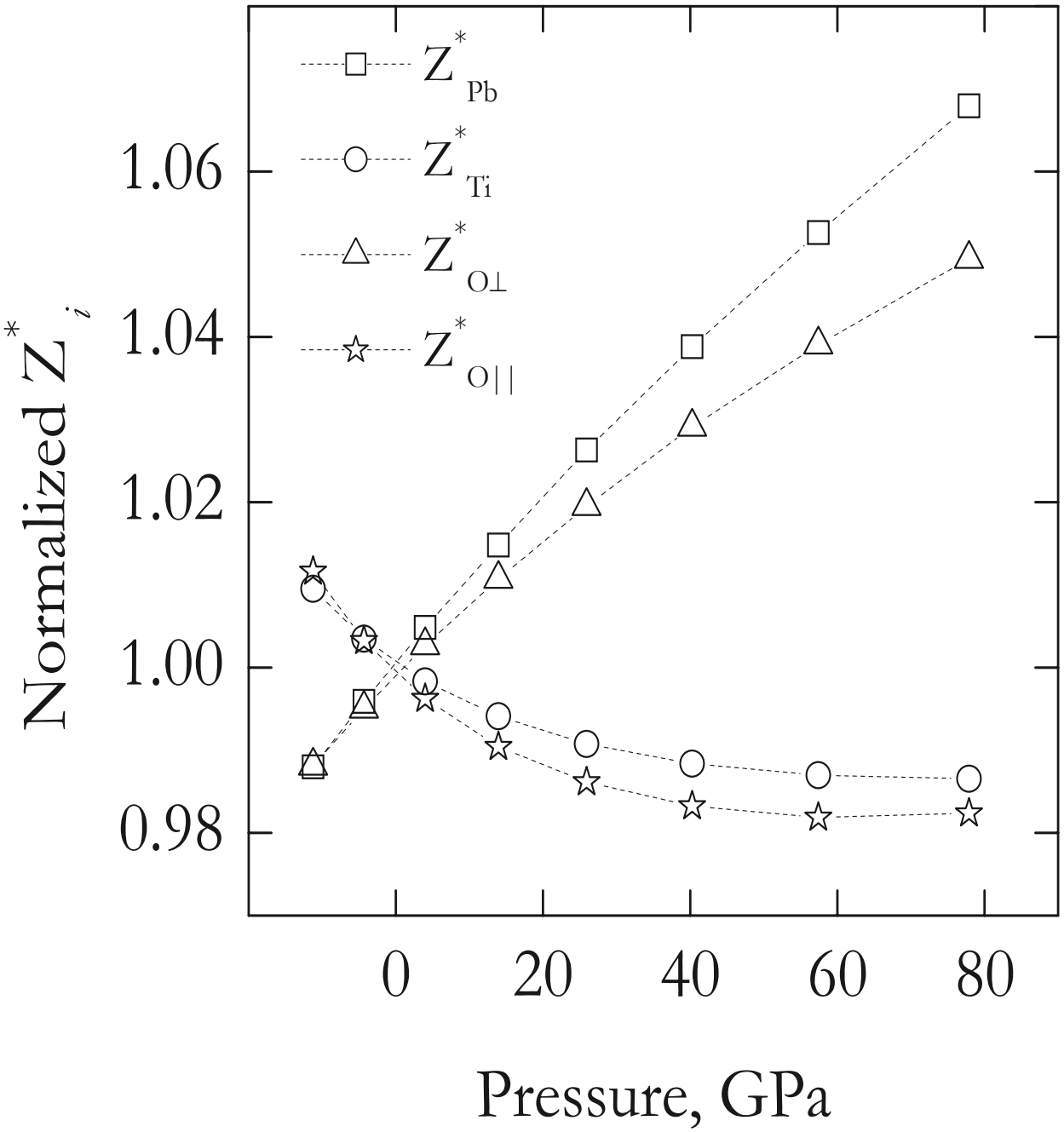

FIG. 4 Pressure evolution of the normalized Born effective charges for Pb, Ti, $O_\perp$ and $O_\parallel$ in the cubic phase of $PbTiO_3$. The normalization is done with respect to the Born effective charges at zero pressure obtained with ABINIT for Pb, Ti, $O_\perp$, and $O_\parallel$ in the cubic $Pm\overline{3}m$ phase – that are 3.915, 7.14, -2.61 and -5.85, respectively.

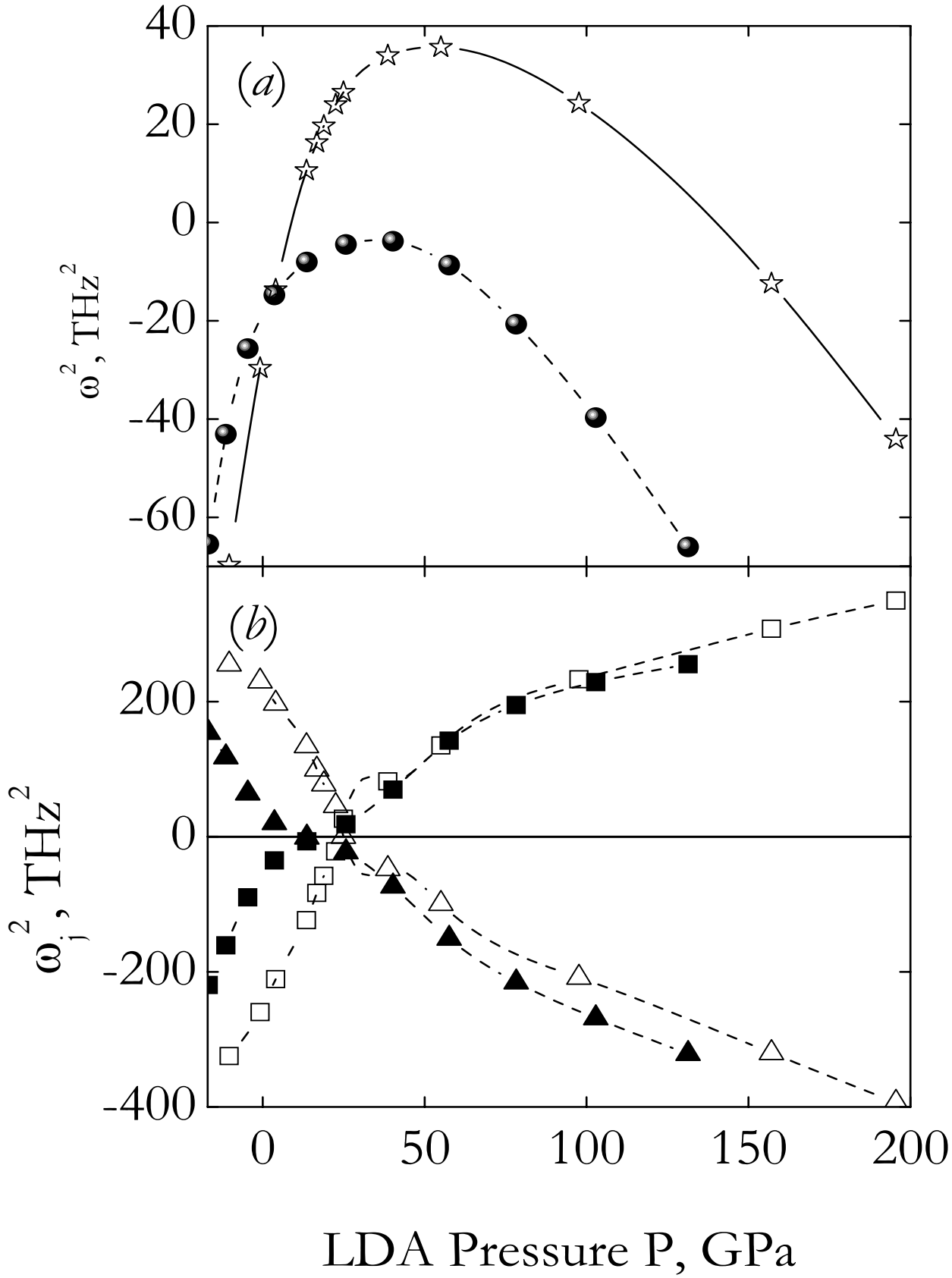

FIG. 5 Pressure behavior of phonons in $PbTiO_3$ (solid symbols) and $BaTiO_3$ (open symbols). Panel (a) displays the square of the zone-center TO phonon frequency in the cubic phase within LDA at 0K. Panel (b) shows the contributions from the Coulomb interactions (squares) within the rigid ions model and non-Coulomb interactions (triangles) to this square.

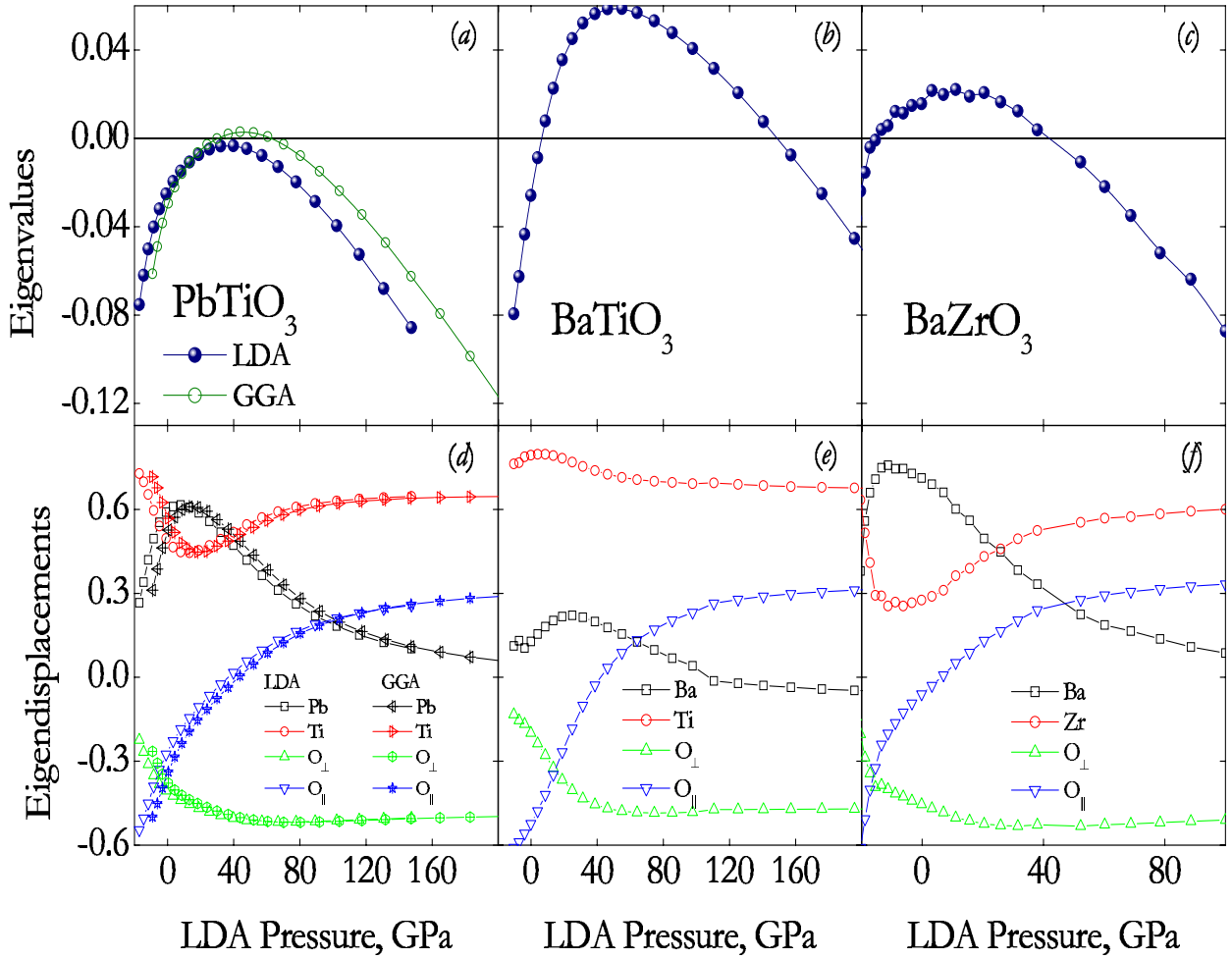

FIG. 6 LDA-predicted pressure behavior of the soft-mode eigenvalue and eigenvectors of the second-derivative matrix in cubic $PbTiO_3$ (panels (a) and (d)), $BaTiO_3$ (panels (b) and (e)) and $BaZrO_3$ (panels (c) and (f)). The GGA results are also shown for $PbTiO_3$ in panels (a) and (d), and suggest that $PbTiO_3$ may be paraelectric within a small pressure range. O_3 is the oxygen atom located between two (slightly displaced) B-atoms along the [001] direction.

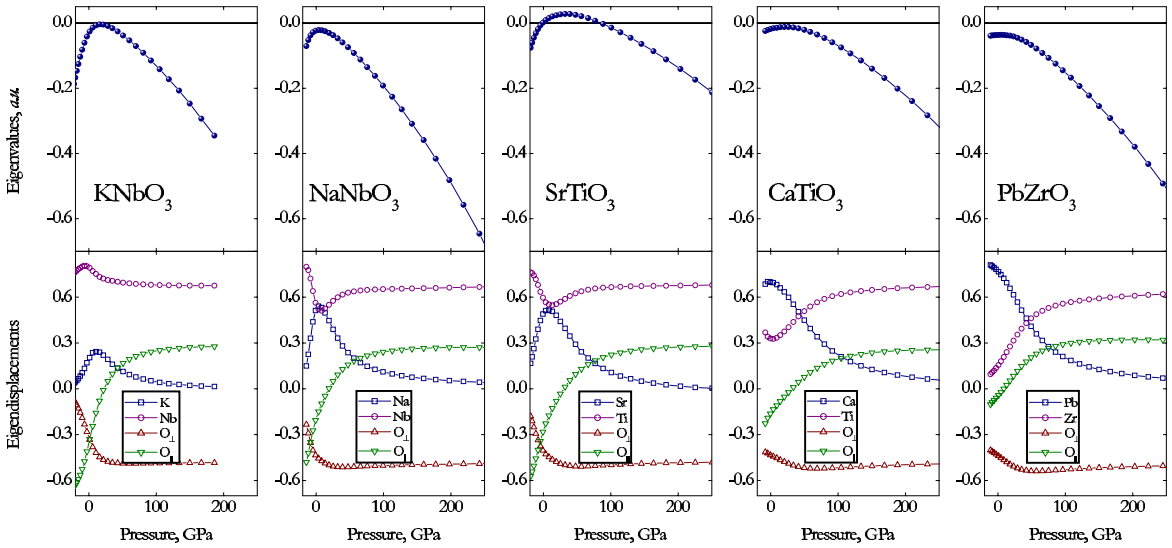

FIG. 7 LDA-predicted pressure behavior of the soft-mode eigenvalue and eigenvectors of the second-derivative matrix in cubic $KNbO_3$, $NaNbO_3$, $SrTiO_3$, $CaTiO_3$ and $PbZrO_3$.

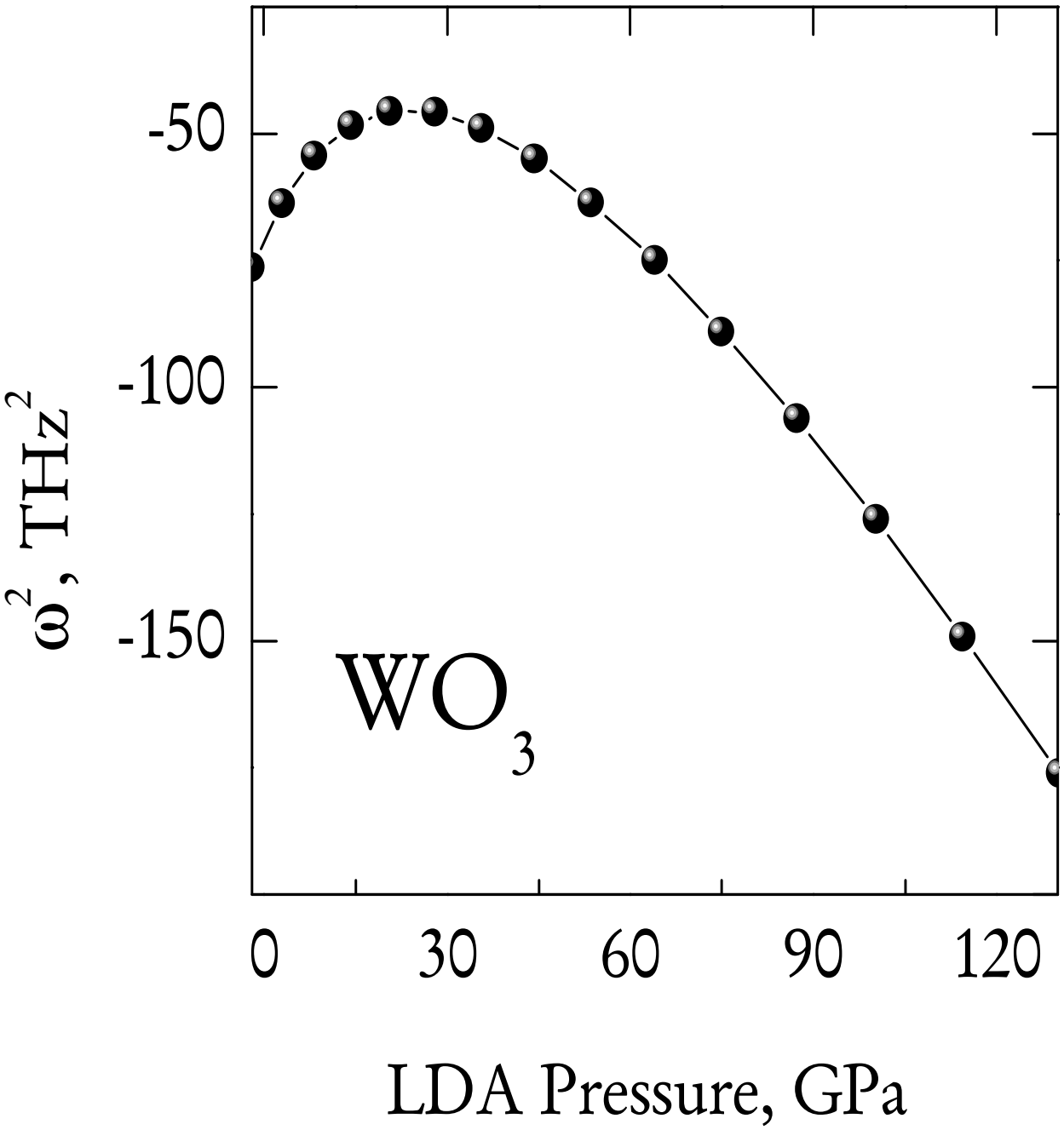

FIG. 8 LDA-predicted pressure behavior of the soft-mode frequency square in cubic WO_3.

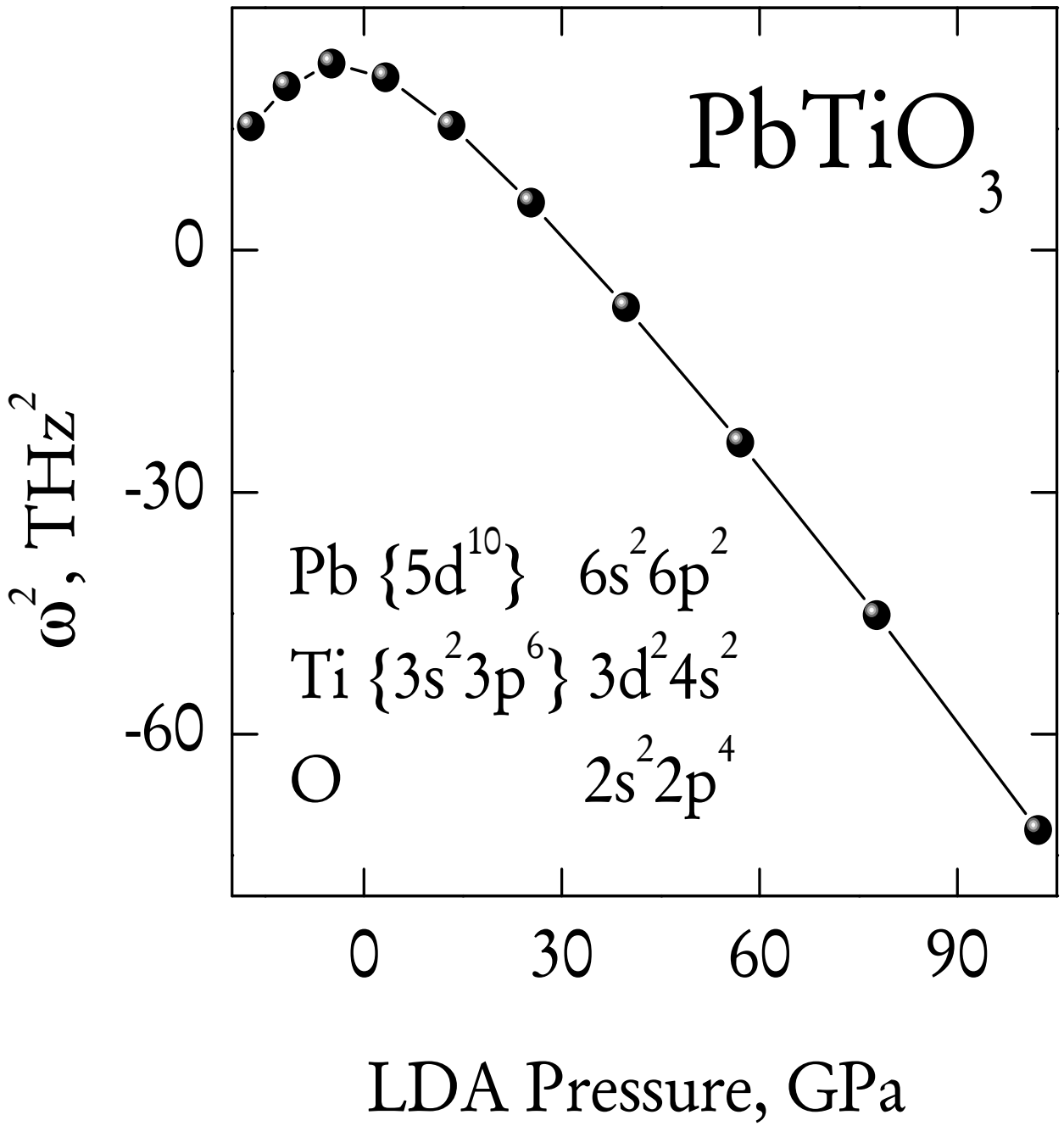

FIG. 9 LDA-predicted pressure behavior of the soft-mode frequency square in the cubic phase of $PbTiO_3$, when excluding the 5d semicore states of Pb and 3s and 3p semicore states of Ti from the valence electrons (unlike the 6s and 6p states of Pb, the 3d and 4s states of Ti and the 2s and 2p states of oxygen that are kept in the valence).

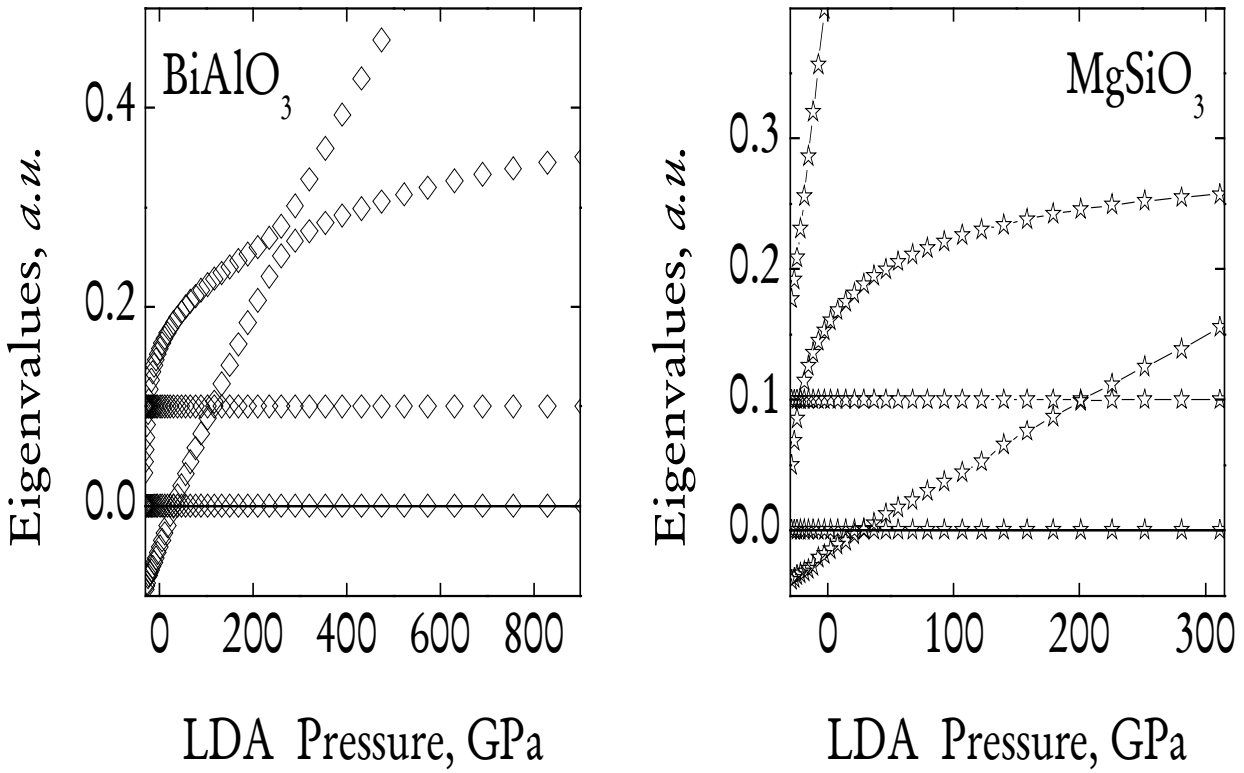

FIG. 10 LDA-predicted pressure behavior of the soft-mode eigenvalues of the second-derivative matrix in cubic bismuth aluminate $BiAlO_3$ and magnesium silicate $MgSiO_3$.

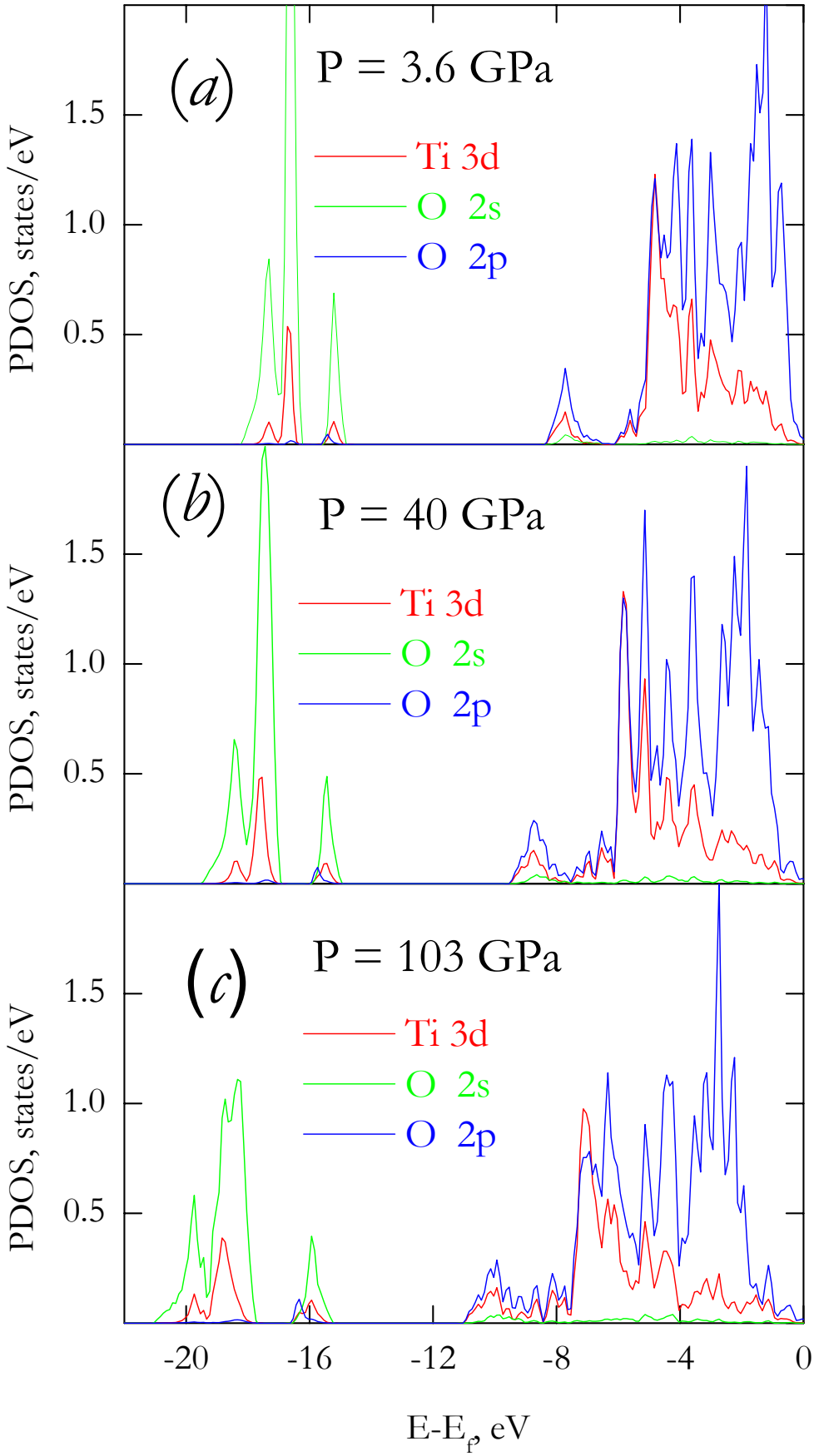

FIG. 11 Electronic-related properties of $PbTiO_3$ under pressure. Panels (a), (b) and (c) display the partial electronic density of occupied states in the cubic phase at 3.6, 40 and 103 GPa, respectively, for the O *2s*, O *2p* and Ti *3d* orbitals. The zero in energy is chosen at the top of the valence band,

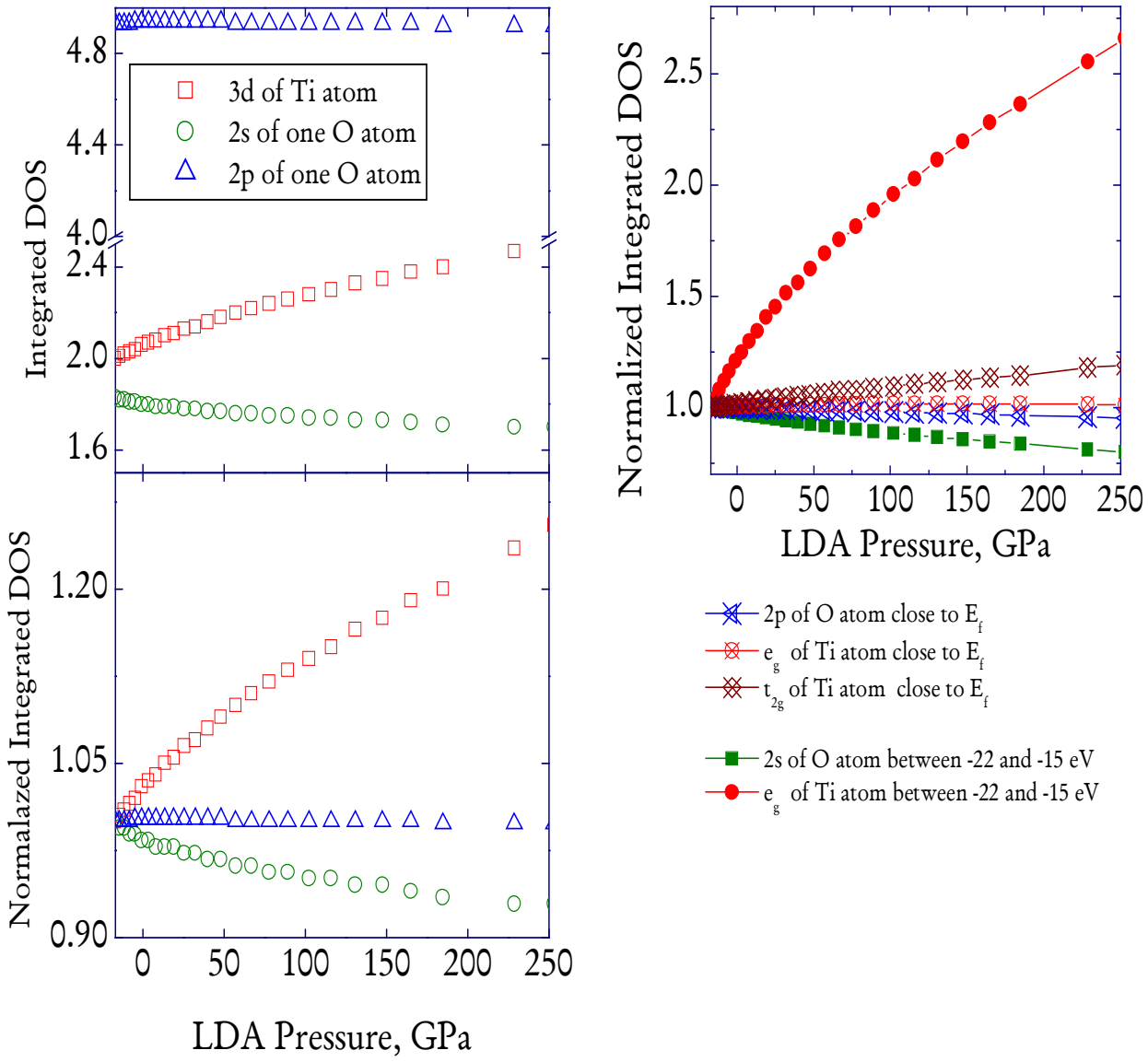

FIG. 12 Integrated DOS of $PbTiO_3$ under pressure in the cubic state. Panel (a) displays the integrated PDOS for Ti *3d* and O *2p* and *2s* states; panel (b) displays the normalized integrated PDOS for the same states; panel (c) displays the contributions to the normalized integrated PDOS coming from the low-lying O *2s* and Ti *3d* e_g states (located between -22 and -15 eV) and from the topmost group of the valence O *2p* and Ti *3d* bands.

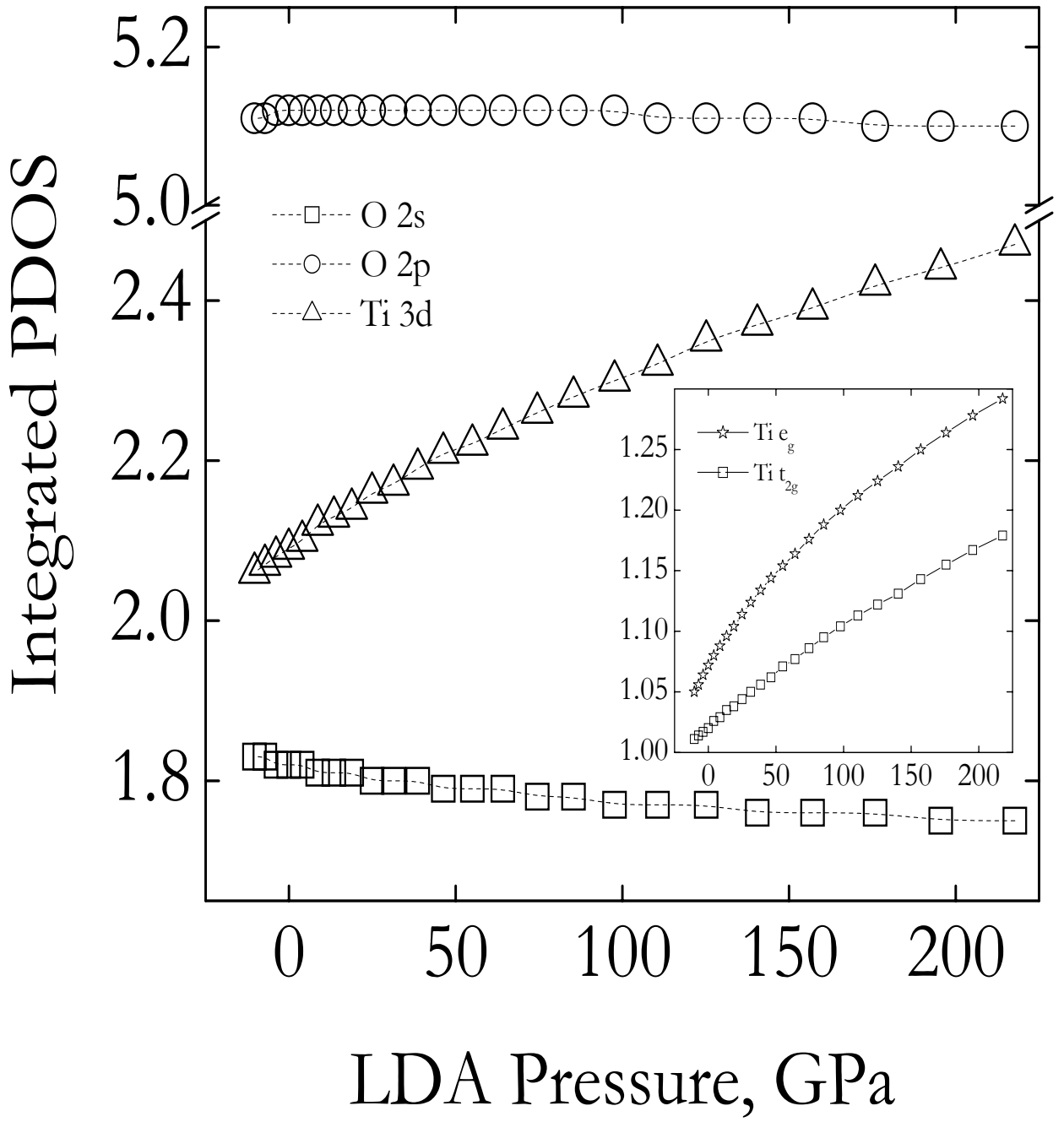

FIG. 13 Integrated PDOS of $BaTiO_3$ under pressure in the cubic state. The inset shows the variation of the integrated PDOS of Ti *3d* e_g and Ti *3d* t_{2g} versus pressure.

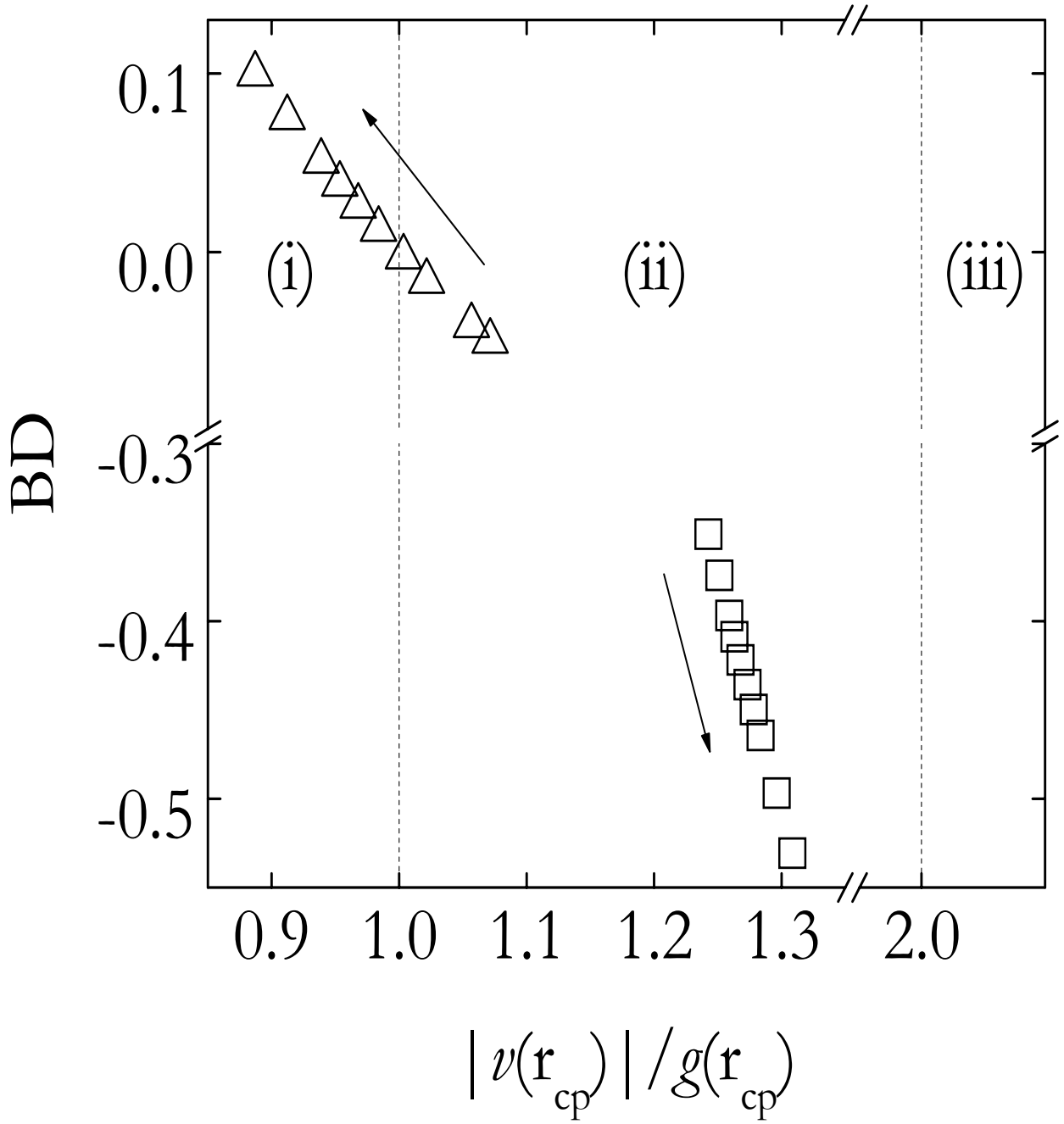

FIG. 14 The bond degree parameter $BD = h(r_{cp})/\rho(r_{cp})$ vs. $|v(r_{cp})|/g(r_{cp})$ ratio for the Ti-O (squares) and Pb-O (triangles) bonds. The arrows indicate the direction of pressure increase. Vertical dashed lines indicate the regions of stability for the three classes of atomic interactions (see text).

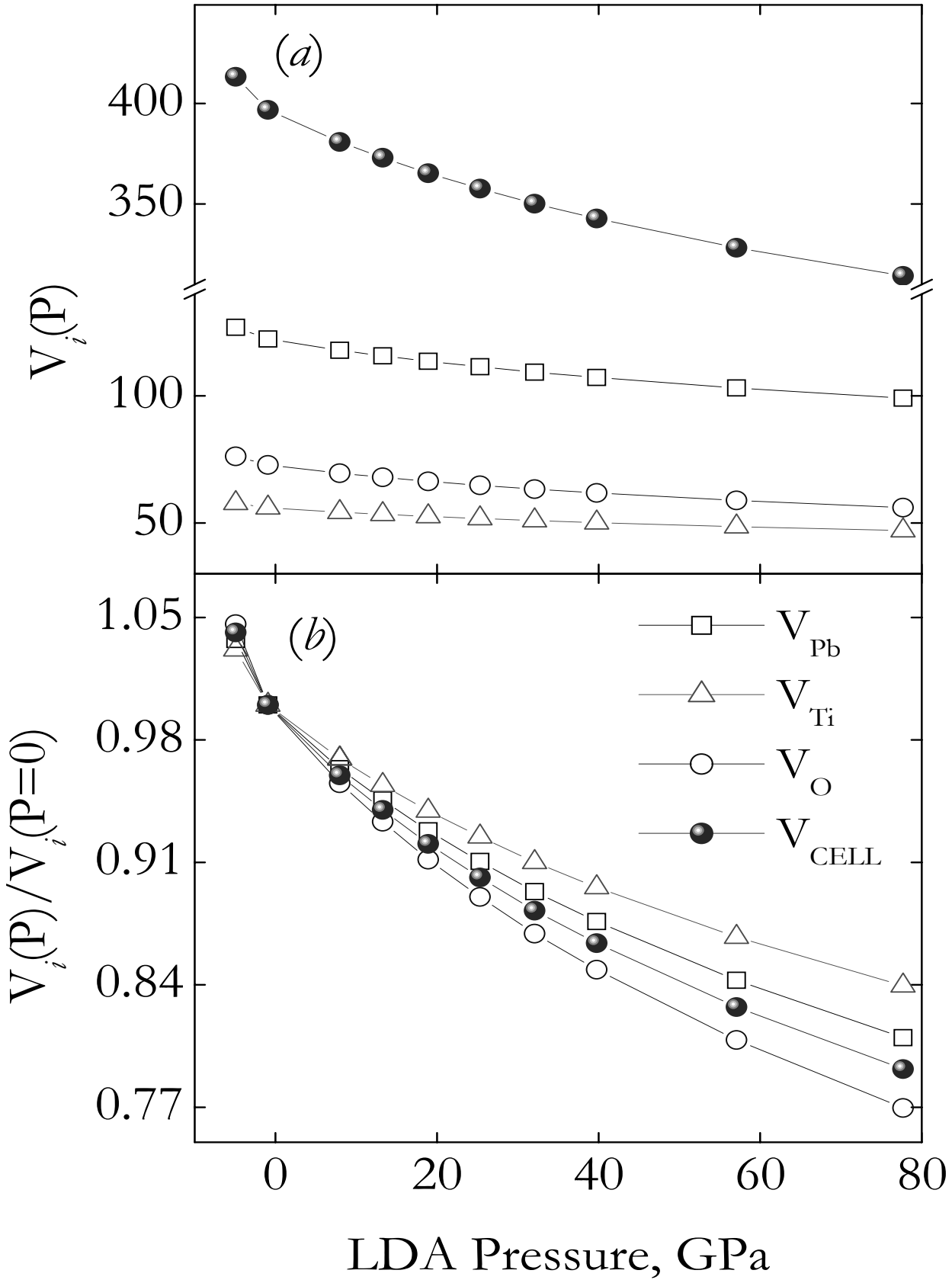

FIG. 15 (a) Pressure evolution of the ionic Bader volumes for Pb, Ti and O and the unit cell volume V_{CELL} in the cubic phase of $PbTiO_3$. (b) The pressure dependence of the normalized volumes. (The normalized volumes are equal to unity at 0 GPa.)

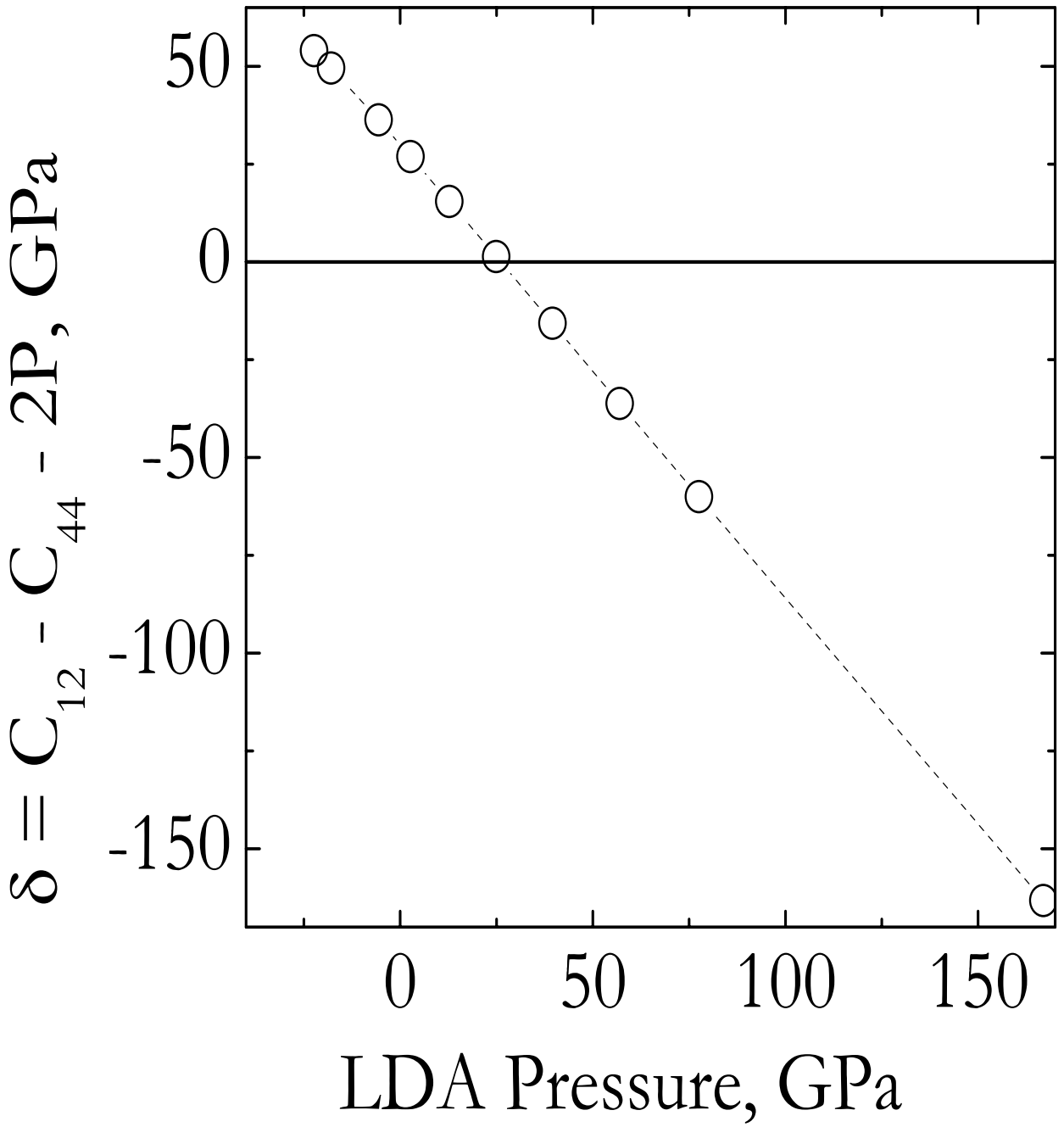

FIG. 16 LDA-predicted deviations from the Cauchy relation ($\delta = C_{12} - C_{44} - 2P$) as a function of pressure for the cubic phase of $PbTiO_3$.

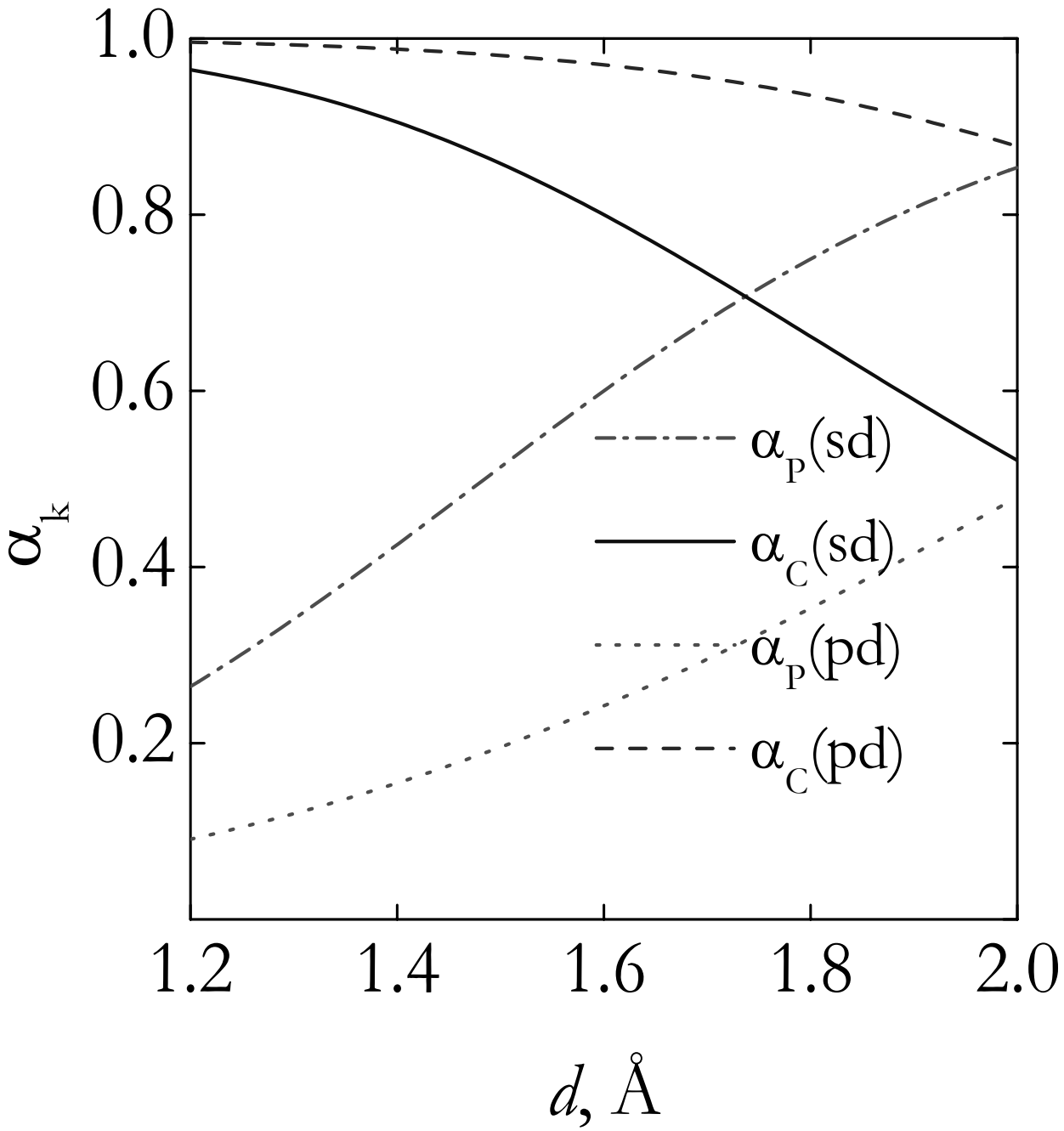

FIG. 17 The Ti3d-O2s and Ti3d-O2p bonds polarity and covalency of a perovskite as a function of the interatomic Ti-O distance d in the ideal cubic phase. (Note that the pressure increases as d decreases).

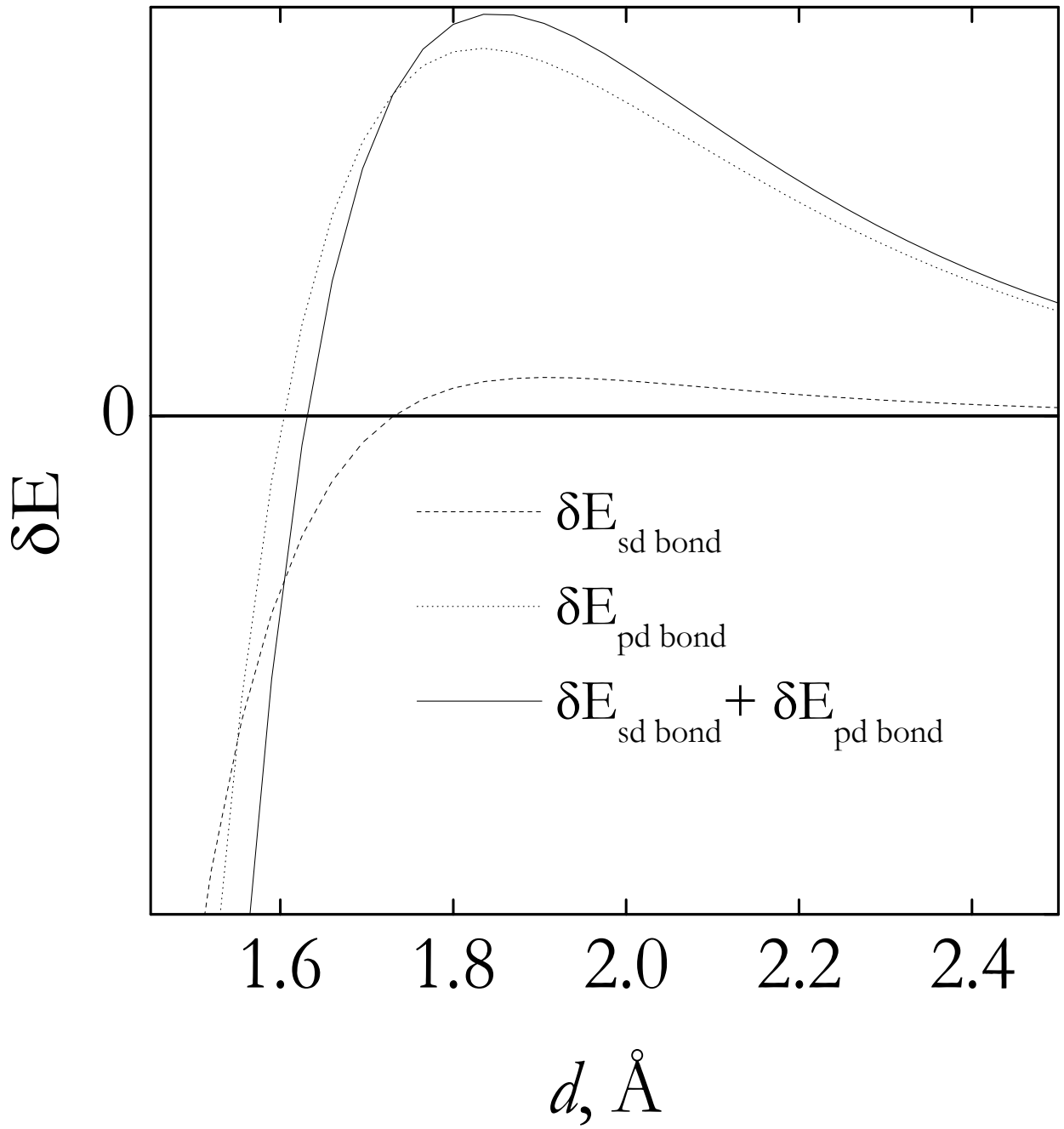

FIG. 18 Change in bonding energy (solid lines) within the bond-orbital model of Harrison. This change is directly proportional to the soft-mode frequency square within this model. The contributions of the *sd* and *pd* bonds to that total change are also indicated via dashed lines. d is the Ti-O distance in the ideal cubic phase.

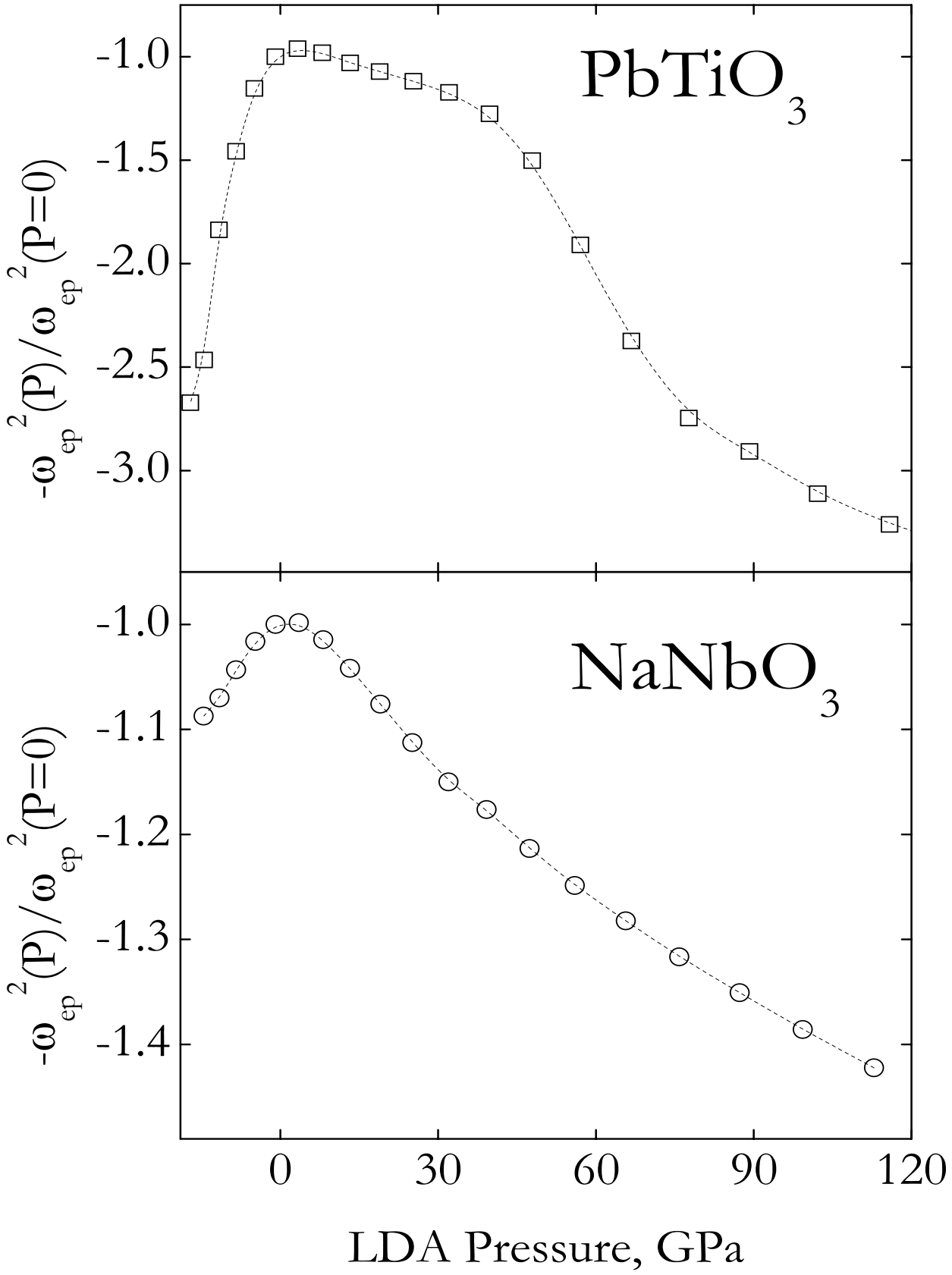

FIG. 19 Normalized electron-phonon contribution ω_{ep}^2 to the ferroelectric soft mode at the Γ point in the cubic state of $PbTiO_3$ and $NaNbO_3$. Normalization has been done such as to obtain values of -1 at 0 GPa.